land

MDPI

Article

Characterization of Land-Cover Changes and Forest-Cover Dynamics in Togo between 1985 and 2020 from Landsat Images Using Google Earth Engine

Arifou Kombate [1,*], Fousseni Folega [2], Wouyo Atakpama [3], Marra Dourma [2], Kperkouma Wala [2] and Kalifa Goïta [1]

1 Centre d'Applications et de Recherches en Télédétection (CARTEL), Département de Géomatique Appliquée, Université de Sherbrooke, Sherbrooke, QC J1K 2R1, Canada
2 Géomatique et Modélisation des Écosystèmes, Laboratoire de Botanique et Écologie Végétale (LBEV), Département de botanique, Faculté des sciences, Université de Lomé, 01 BP 1515 Lomé, Togo
3 Unité de Recherche en Systématique et Conservation de la Biodiversité, Laboratoire de Botanique et Écologie Végétale (LBEV), Département de botanique, Faculté des sciences, Université de Lomé, 01 BP 1515 Lomé, Togo
* Correspondence: arifou.kombate@usherbrooke.ca

check for updates

Citation: Kombate, A.; Folega, F.; Atakpama, W.; Dourma, M.; Wala, K.; Goïta, K. Characterization of Land-Cover Changes and Forest-Cover Dynamics in Togo between 1985 and 2020 from Landsat Images Using Google Earth Engine. *Land* **2022**, *11*, 1889. https://doi.org/10.3390/land11111889

Academic Editors: Carmine Serio, Guido Masiello and Sara Venafra

Received: 2 September 2022
Accepted: 21 October 2022
Published: 25 October 2022

Abstract: Carbon stocks in forest ecosystems, when released as a result of forest degradation, contribute to greenhouse gas (GHG) emissions. To quantify and assess the rates of these changes, the Intergovernmental Panel on Climate Change (IPCC) recommends that the REDD+ mechanism use a combination of Earth observational data and field inventories. To this end, our study characterized land-cover changes and forest-cover dynamics in Togo between 1985 and 2020, using the supervised classification of Landsat 5, 7, and 8 images on the Google Earth Engine platform with the Random Forest (RF) algorithm. Overall image classification accuracies for all target years ranged from 0.91 to 0.98, with Kappa coefficients ranging between 0.86 and 0.96. Analysis indicated that all land cover classes, which were identified at the beginning of the study period, have undergone changes at several levels, with a reduction in forest area from 49.9% of the national territory in 1985, to 23.8% in 2020. These losses of forest cover have mainly been to agriculture, savannahs, and urbanization. The annual change in forest cover was estimated at −2.11% per year, with annual deforestation at 422.15 km^2 per year, which corresponds to a contraction in forest cover of 0.74% per year over the 35-year period being considered. Ecological Zone IV (mountainous, with dense semi-deciduous forests) is the one region (of five) that has best conserved its forest area over this period. This study contributes to the mission of forestry and territorial administration in Togo by providing methods and historical data regarding land cover that would help to control the factors involved in forest area reductions, reinforcing the system of measurement, notification, and verification within the REDD+ framework, and ensuring better, long-lasting management of forest ecosystems.

Keywords: land-cover change; REDD+; Google Earth Engine; random forest; landsat; Togo

1. Introduction

Forests contribute greatly to soil conservation and climate change mitigation and represent one of the simplest and most effective means of establishing or maintaining carbon sinks [1]. As one of the most important global carbon reservoirs, tropical forests are home to between half and two-thirds of the Earth's species [2]. Unfortunately, these forest carbon stocks are not stable, given that conversion to other land cover is occurring at an alarming rate despite the increased awareness of climate change [3,4]. Between 2000 and 2005, land-use and land-cover (LULC) changes resulted in forest cover reductions of 0.6% per annum worldwide [5]. Between 2015 and 2020, annual deforestation rates were estimated at 10 million hectares globally [6]. Such land-cover changes occur mainly as a result of anthropogenic disturbances, including deforestation, together with the expansion of croplands and urban areas [7]. LULC changes, mostly caused by agriculture and deforestation, contribute to about one-third of global greenhouse gas (GHG) and worsen the adverse effects of climate change [8,9]. Faced with these increasingly significant effects of climate change, ongoing demands for action are becoming more urgent to curb the extent of deforestation and forest degradation, while enhancing carbon storage through better accounting of carbon sources and sinks. To this end, the United Nations Framework Convention on Climate Change (UNFCCC) has established the REDD+ (Reducing Emissions from Deforestation and forest Degradation Plus) mechanism, which is seen as a global system of centralized forest governance. Aimed primarily at developing nations, REDD+ provides financial compensation for these countries to preserve their forests to reduce carbon emissions and, thus, mitigate the risks of climate change [10,11].

In order to qualify for financial offsets by implementing REDD+, these countries are required to establish National Measurement, Reporting, and Verification (MRV) systems within a national forest monitoring system (NFMS) that must provide national estimates of changes in forest carbon stocks and emissions every two years. The Intergovernmental Panel on Climate Change (IPCC) recommends a combination of Earth observation data and field inventories to estimate forest area, carbon stocks, and changes that follow disturbance [12]. Regular analysis of forest dynamics and LULC changes using satellite data could effectively establish the baseline for the MRV reporting requirement in this context. However, many concerned developing countries are generally faced with a lack of quantitative data on forest degradation-induced changes and limited technical capabilities and material capacity to produce such data for GHG emissions monitoring [12].

The aforementioned challenges beset the West African nation of Togo (République Togolaise), which is the subject of our study, in its quest to meet reporting requirement needs within the framework of the REDD+ strategy, and to guide strategies for monitoring the evolution of forest ecosystems and land cover. A few studies based on observational data have made it possible to monitor changes in land cover in certain parts of the country, but they generally have a starting and an ending year for a period that occasionally spans several decades. The coarse temporal frequency of sampling does not make it possible to detect changes that have been incurred within these periods or to discern which main factors drive their behavior. Furthermore, the spatial extent of these studies is often very limited (i.e., river basins, protected zones, and administrative jurisdictions, among others), whereby changes are not perceived across an entire ecological region or on a national scale. Land and vegetation cover have been studied, but these changes are mainly in protected areas [13–16]. Other studies have focused on watersheds [17,18], while some have been carried out at regional or prefectural scales [19,20]. To a much lesser extent, few comprehensive studies have spanned several ecological zones [21]. These studies have generally covered about 1 to 10% of the national territory, and there are regrettably very few studies quantifying the LULC changes observed over time or analyzing the drivers of these changes.

The spatial and temporal limitations of these previous studies in detecting land-cover changes are related to the difficulties in finding sufficient cloud-free satellite images over large areas. This problem could be overcome by using Synthetic Aperture Radar (SAR) images which, even when acquired in all atmospheric and solar conditions, allow change detection analyses [22], but SAR long historical data does not exist in our study area. These limitations are also related to computational resource problems (large storage capacity and access to high computing power), together with the labor-intensive nature of processing these mega-data [23,24]. Furthermore, global-scale mapping projects often use satellite data with a variable spatial resolution (1 km to 30 m), and generally do not involve local experts; therefore, these approaches do not meet the standards of accuracy that are sought at the national level [25]. With the availability of the new geospatial technology of the Google Earth Engine (GEE), it is now possible to apply very advanced machine-learning algorithms in an efficient manner [26]. The GEE is a cloud-computing platform with a JavaScript code editor that integrates a long-time series of satellite imagery, thereby allowing the classification of large volumes of data and the production of multi-date land-cover changes. It should be further noted that relatively few studies in the scientific literature have focused on the use of these methods to advance operational forest monitoring in MRV systems [27].

The major challenges to implementing Togo's national REDD+ strategy are reversing the process of forest degradation and savannization, while spatially containing agricultural pressure and constraining urban expansion. These measures should eventually increase carbon stocks and reduce greenhouse gas emissions [28]. Unfortunately, most studies that have been conducted in Togo on progressive LULC changes are incomplete, and forest inventories over the last three decades are very limited. The availability of historical LULC data at a national scale is necessary to meet the challenge of better understanding the LULC dynamics and forest developmental trends over time. This study aims to answer the question of whether the use of multi-temporal images in the GEE would provide a picture of land-cover changes, particularly forest cover, at the national scale. Its main objective is to characterize vegetation dynamics over the entire national territory using a long-time series of Landsat images from 1985 to 2020. More specifically, the study aims to quantify the evolution of spatiotemporal changes and to analyze their effects on forest cover during this period.

2. Study Area and Data Used

2.1. Study Area

The study area was Togo (Figure 1A). It is a coastal country in West Africa that is bordered by Burkina Faso to the north, the Atlantic Ocean to the south, Benin to the east, and Ghana to the west. It belongs to the Sudano-Guinean zone, which is a climatic zone that is located south of the Sahara Desert in the continental and coastal areas, which extend from West Africa to Central Africa. With an area of 56,600 km^2, Togo has a population of 7,264,637 inhabitants unequally distributed in the administrative regions with proportions of 42.16% in Maritime, 22.16% in Plateaux, 9.99% in Centrale, 12.44% in Kara and 13.26% in Savanes [29]. It experiences a tropical Sudano-Guinean climate with rainfall ranging from 900 to 1100 mm year^{-1} in the northern regions (distinct wet and dry seasons), and from 1000 to 1600 mm year^{-1} in the southern regions (with four seasons), and an average temperature of 27 °C [30].

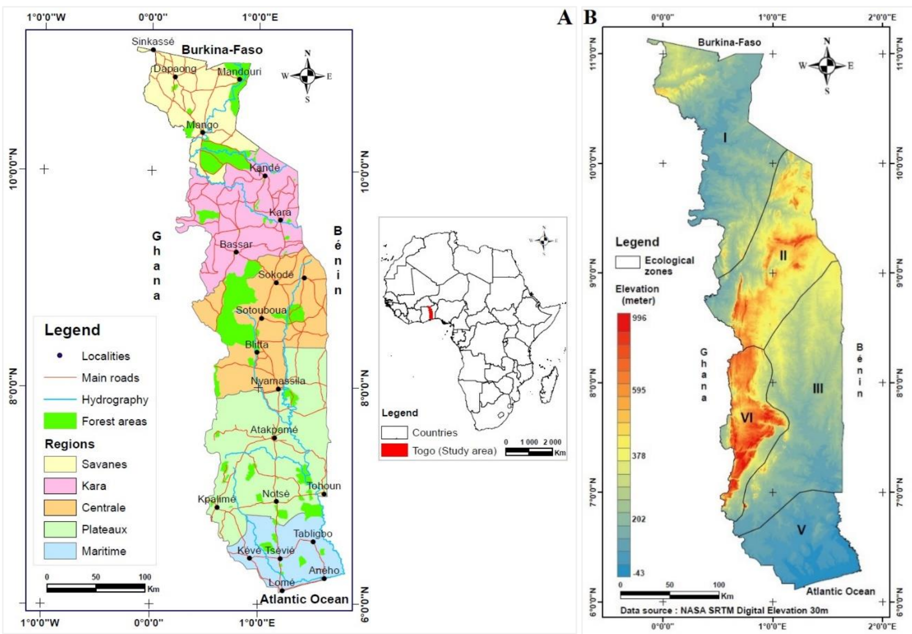

Figure 1. (**A**) Geographical location of the study area; (**B**) ecological zones and elevations.

Due to its position in the Dahomey Gap (a remarkable interruption in the extent of continuous tropical rainforest covering Central to West Africa), Togo has a low forest cover with a deforestation rate of 0.73% per year for the period from 1990 to 2000 [31]. To ensure the protection of the country's forest resources, 14.2% of its territory was classified between 1939 and 1957 as 83 protected areas (classified forests, national parks, and reserves). Yet, human populations seeking arable land and wood for energy have encroached upon nearly one-third of these areas [32]. Vegetation formations are composed of the Sudano-Guinean forest that is located in the mountainous areas of the country, gallery forest along main rivers, dry forest or dense tree savannah in the northern half, and tree savannah in the south and center. The landscape variability of these ecosystems led [33] to subdivision of the country into five ecological zones (Figure 1B).

Ecological zones correspond to distinct ecosystems that are characterized by various plant formations and topographies. Following an update of their descriptions, these ecological zones have been summarized in [34] as follows:

- Zone I (or Northern Plains Zone): This zone extends from the Dapaong peneplain to the southern limit of the Volta Basin, approximately following the Bendjeli-Kpessidè axis. This area is essentially dominated by agro-ecosystems; however, there are relic mosaics of savannahs, dry forests, degraded riparian forests, and swamp vegetation adjacent to the hydrographic network. The main spontaneous ligneous species found in this zone are *Vitellaria paradoxa*, *Anogeisus leiocarpus*, *Borassus aethiopum*, *Parkia biglobosa*, *Balanites aegyptiaca*, *Lannea microcarpa*, and *Detarium microcarpa*. The natural ecosystems of this area are highly degraded (80%), given the strong propensity of the inhabitants to practice unsustainable cultivation (68%) and fuel wood exploitation (28%). The zone is heavily disturbed by vegetation fires (40%), which have then been followed by extensive grazing (28%) [34].
- Zone II (or Northern Mountains Zone): This zone encompasses the Northern Mountain Range and extends between 8° and 10° N northeast under the influence of a Sudanian mountain climate. This zone is dominated by agrosystems, yet dry forests, open forests, and savannah mosaics can be found. Its main spontaneous ligneous species are *Parkia biglobosa*, *Vitellaria paradoxa*, *Nauclea latifolia*, *Daniellia oliveri*, *Elaeis guineensis*, *Piliostigma thonningii*, *Terminalia laxiflora*, and *Isoberlinia doka*. In this zone, natural ecosystems are also degraded (58%) and heavily disturbed by extensive grazing (31%), followed by vegetation fires (25%), floods (19%), and transhumance (seasonal livestock relocation, 17%). Activities such as working crop fields (41%), logging (22%), and grazing (20%) strongly contribute to ecosystem degradation [34].
- Zone III (or Central Plains Zone): This zone occupies the Benin-Togolese plain east of the Atakora Mountain Chain; it is characterized by a Guinean Lowland climate and is dominated by a diversity of agrosystems. This matrix of agroforestry parks combines patches of mosaic savannah, semi-deciduous forest, and degraded riparian formations. This zone is characterized by the following main spontaneous ligneous species: *Daniellia oliveri*, *Parkia biglobosa*, *Vitellaria paradoxa*, *Pterocarpus erinaceus*, *Anogeissus leiocarpus*, and *Adansonia digitata*. The natural ecosystems of this agro-ecological zone are 96% degraded. This degradation of ecosystems is the consequence of the exploitation of wood energy (46%) and cultivation practices (41%) and is not very sustainable. Ecosystems in this zone are strongly disturbed by vegetation fires (31%), transhumance (31%), and erosion (24%) [34].
- Zone IV (or Southern Zone of the Togo Mountains): This zone corresponds to the southern portion of the Togo Mountains. It has a sub-equatorial climate with a rainy season. Its main spontaneous ligneous species are *Cola gigantea*, *Millettia thoningii*, *Morinda lucida*, *Sterculia tragacantha*, *Antiaris fricana*, *Holarrhena floribunda*, and *Margaritaria dioscoidea*. Today, it is the domain par excellence of agroforestry that is interspersed with semi-deciduous forests and mosaics of Guinean savannah. The natural ecosystems of the southern zone of the Togo Mountains are highly degraded (70%), given that they are heavily disturbed by vegetation fires (55%), often followed by extensive grazing (15%),

and logging (10%). Activities such as working the crop fields (59%) and logging (18%) contribute to the substantial degradation of ecosystems [34].

- Zone V (or Southern Coastal Zone): This zone corresponds to the country's coastline with a sub-equatorial climate with two rainy seasons. The very degraded natural environment is strongly dominated by agrosystems, with relic mosaics of savannahs, halophytic or swampy grasslands, and mangroves. The main spontaneous ligneous species found there are *Lonchocarpus sericeus*, *Parkia biglobosa*, *Piliostigma thonningii*, *Dialium guineense*, *Holarrhena floribunda*, *Bridelia ferruginea Millettia thonningii*, and *Vitellaria paradoxa*. These natural ecosystems are highly degraded (85%) due to cultivation practices (59%) and the unsustainable exploitation of wood energy (18%) and urbanization (10%). Lands in the Coastal Zone have been heavily disturbed by vegetation fires (55%), which are often followed by extensive grazing (15%), and transhumance, woodcutting, and flooding (5%) [34].

The aforementioned descriptions indicate the continuation of high-intensity land degradation that has been observed across most of these zones since the 1990s [35]. Even in Zone IV, which is known as being the most extensively forested of the ecological zones, deforestation and forest degradation have been occurring in recent years due to the combined effect of the advancing agricultural front with slash-and-burn agriculture, wildfires, and logging [36].

2.2. Data Used

Data used in this study included Landsat TM, ETM+ (Enhanced Thematic Mapper Plus), OLI (Operational Land Imager) satellite imagery, land-cover reference data, and vector data. The satellite images are from Landsat 5, 7, and 8 sensors with a spatial resolution of 30 m, which have been archived in the GEE (Table 1). Image selections were made for the level-1 scenes, which are the best quality images in terms of radiometric consistency and atmospheric correction [37]. These are surface reflectance data that were accompanied by meta-data and per-pixel quality information, which was intercalibrated between different Landsat sensors, and are considered suitable for time-series processing analysis [38].

Table 1. Information on Landsat images that were entered into composites from 1985 to 2020.

Sensors	Composite Target Years	Composite Image Acquisition Period	Admissible Cloud Threshold	Number of Images that Were Concerned
Landsat 5	1985	1983-01-01 to 1986-12-31	10%	57
Landsat 5	1990	1987-10-01 to 1988-03-31 1988-10-01 to 1989-03-31 1989-10-01 to 1990-03-31 1990-10-01 to 1991-03-31 1991-10-01 to 1992-03-31 1992-10-01 to 1992-12-31	10%	49
Landsat 7	2000	1999-04-16 to 2002-12-31	10%	95
Landsat 7	2005	2003-01-01 to 2007-12-31	20%	322
Landsat 8	2015	2013-01-01 to 2017-12-31	10%	265
Landsat 8	2020	2018-01-01 to 2020-12-31	10%	171

Land cover reference data consisted of data that were collected in the field, points that were sampled on image composites, and high-resolution Google Earth images. During the field campaign that was conducted from October 2020 to February 2021, we sampled 101 land occupancy points on the ICESat (Ice, Cloud, and land Elevation Satellite) data footprints, 303 points on the ICESat-2 data footprints, and 114 points elsewhere. These ICESat and ICESat-2 footprint data are dendrometric data that are intended for further studies on estimating aboveground biomass. Given that the land occupancies of these sites were known, they were used with other data as references for training and validation of classifications that were made during this study. Vector data mainly concerned forest areas, administrative regions, ecological zones, and jurisdictional boundaries in Togo. Large-scale international boundary data for Togo (i.e., the study area) that were also available in the GEE were used for delineation during the selection of these images and the final mapping.

3. Methodology

The methodological approach of this study involved the acquisition and pre-processing of satellite data, selection of training and validation data, supervised classification of the images with the Random Forest (RF) algorithm, evaluation of classification accuracies, and mapping and analysis of the results. The following flowchart (Figure 2) illustrates the methodological approach which is summarized in three main points in the description.

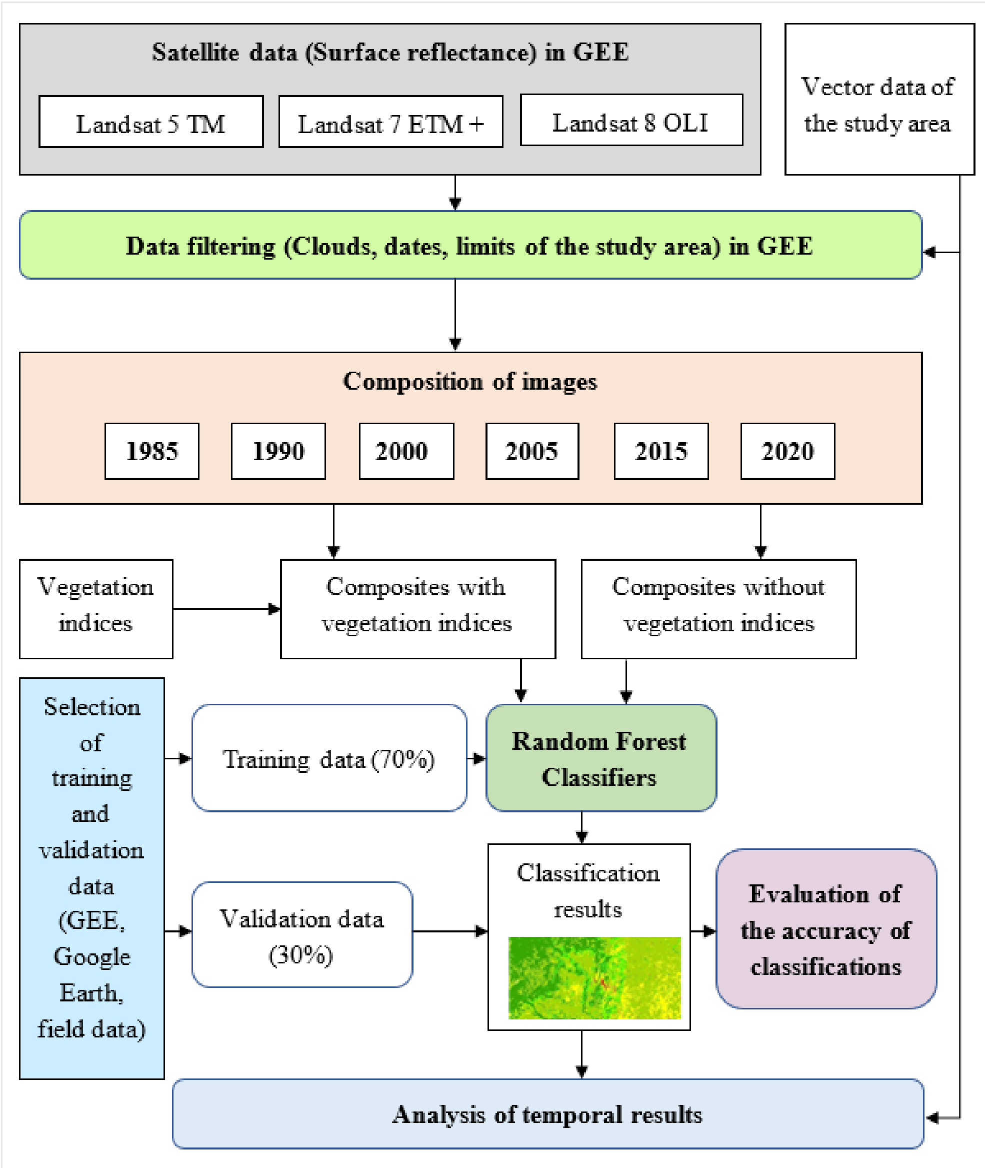

Figure 2. Methodological flowchart of the study.

3.1. Selection and Pre-Processing of Satellite Images

Since cloud-free images providing complete coverage of the study area for the target year were difficult to find, image composition was performed. This consisted of filtering all images with admissible cloud cover set to a certain threshold (Table 1) to create a mosaic of images around each target year. Referring to methods that are frequently used in the literature, several authors had performed image composition based on the temporal aggregation of data, applying the calculation of statistical parameters (mean, median, and maximum or minimum values) on the pixels of a pre-defined image time series [39,40]. Others simply used all available Landsat images in their study area to compose image time series [41,42]. According to [24], the most popular strategy for selecting input images for an annual cloud-free composite is using images that have been acquired over three years. In this study, the annual data composite was targeted from the year 1985, with a five-year step to better perceive disturbance lapse times. Unfortunately, there were problems of poor quality and insufficiently filtered images below the set cloud thresholds, together with gaps in the data covering the study area. Faced with these difficulties, only six image composites were created, from all available data in the target years, or occasionally, one or two years on either side of the target years (i.e., 1985, 1990, 2000, 2005, 2015, and 2020). Image composites were formed by applying a cloud mask *QA_PIXEL Bitmask* (provided with the data) to the image collections. Cloudy pixels were maintained (by removing the mask) when no other non-cloudy pixels were available to replace them from the entire time period around the target years. These were placed into the cloud class so that the entire extent of the study area could be considered when facilitating later surface analyses. We initially composited these images only from the best-available pixels derived from Landsat data [43]. Nevertheless, given that some parts of the area remained without data under the constraints of the filters, we calculated the median of all pixels that met these imposed filters.

Several vegetation indices were also calculated and added as bands to the image composites to see what improvements they could bring to the classification process. These were NDVI, NDBI, NDWI, and BSI (Table 2).

Table 2. Formulas of the used vegetation indices.

Acronym	Designation	Equation	References
NDVI	Normalized Difference Vegetation Index	$\frac{\rho_{NIR}-\rho_R}{\rho_{NIR}+\rho_R}$	[44,45]
NDBI	Normalized Difference Built-up Index	$\frac{\rho_{SWIR1}-\rho_{NIR}}{\rho_{SWIR1}+\rho_{NIR}}$	[46,47]
NDWI	Normalized Difference Water Index	$\frac{\rho_G-\rho_{NIR}}{\rho_G+\rho_{NIR}}$	[48,49]
BSI	Bare Soil Index	$\left[\frac{(\rho_{SWIR1}+\rho_R)-(\rho_{NIR}+\rho_B)}{(\rho_{SWIR1}+\rho_R)+(\rho_{NIR}+\rho_B)}\right]$	[50,51]

Note: ρ_R, ρ_G, ρ_B, ρ_{NIR}, and ρ_{SWIR1} represent the reflectance of red, green, blue, near-infrared, and short-wave infrared bands, respectively.

Since the study area was characterized by major land-cover classes, including vegetation (dense dry forest, open forest, and savannah), crops and fallow land, buildings and bare soil, and water bodies, we selected these vegetation indices to better characterize them. NDVI has been widely used over many decades to monitor vegetation dynamics in terrestrial ecosystems and remains the most popular index that is used for vegetation assessment [52,53]. Using NIR and SWIR bands, NDWI is commonly and successfully used in the detection and mapping of surface water bodies [54] and the improvement of terrain illumination differences and atmospheric effects. Furthermore, the BSI has been proposed as a more reliable estimator of vegetation status where vegetation covers less than half of an area [51,55]. Ref. [56] has shown that combining NDVI, NDWI, and NDBI data could refine several aspects of urban features and appearance while removing cloud-related noise in image classifications. Based upon these findings, these indices were combined with the classic bands of Landsat data, given that the former are expected to contribute to the development of a more nuanced classification scheme [57]. Using the vector data, the resulting image composites were then clipped with the study area to limit processing within this area.

3.2. Selection of Training and Validation Data

For each target year, sample points were selected based on the land cover that was detected through visual interpretation or by relying upon archival high-resolution Google Earth data from periods as close as possible to the target years. Reference data was collected from various sources for the different target years. For the year 2020, we used data collected in the field as explained in Section 2.2. Reference data based on high-resolution archive images mainly concerned the years 2000, 2005, and 2015. For the years 1985 and 1990, when high-resolution images were not available on Google Earth, we relied on samples of land cover directly collected by visual interpretation on filtered Landsat images of these years. In addition to these data, the pixel values of the added vegetation indices bands were used to guide the selection of samples. Therefore, both visual interpretation and consultation of the pixels that were provided by these additional vegetation indices bands were used to make these selections.

In applying these sample selection methods to image composites of the target years 1985, 1990, 2000, 2005, 2015, and 2020, a total of 1007, 1102, 1219, 1278, 1372, and 1521 points were sampled per composite, respectively, to serve as training points. Each group of points represented the different land cover types. For the six target years, 7499 sample points were thus collected, some to serve as training samples (70%) during the classification of the composite images, and the remainder to validate the classification results (30%).

3.3. Image Classification and Evaluation of Accuracy

Following the identification and pre-processing of images, we proceeded to classify the image composites with the classic Landsat bands, followed by a second classification with these same bands to which were added the vegetation indices to determine their effect on the quality of these classifications. As for the pre-processing, image classifications were performed using JavaScript codes in the GEE. For the selection of the appropriate classification method, several classification algorithms related to supervised machine learning have been used in the literature. These include Support Vector Machines (SVM), Classification and Regression Trees (CART), Stepwise Multiple Linear Regression (SML), and Random Forests (RF). We determined that supervised machine learning classifiers, such as Classification and Regression Trees (CART) and Random Forests (RF), were the most frequently used for this purpose. Furthermore, the use of RF classifiers leads to greater classification accuracy, even when applied to the analysis of data with higher noise levels [58–60]. This is confirmed in studies by [61], who evaluated 179 relevant classifiers from 17 families using 121 datasets. The authors concluded that RF provided the best classifiers. Therefore, we selected the RF algorithm because it yields results with excellent accuracies and can work efficiently on large datasets [62].

The different image composites that resulted from filtering according to the previously mentioned parameters were then classified in the GEE using the RF algorithm. The number of decision trees that were selected for this algorithm was made with reference to the literature, which generally indicates that the greater the number of trees, the better the results. According to [63], it is unclear whether the number of trees should simply be set to the largest computationally manageable value or whether a smaller number of trees might be sufficient or provide better results. [64] compared the performance of the RF model with different numbers of trees on 29 datasets and noted that a forest with 512 trees performs better than one with 1024 trees. They concluded that forest performance does not always improve substantially as the number of trees increases beyond a certain level. While it is commonly thought that tuning hyper-parameters can improve RF performance, [65] acknowledged that improvements achieved by adding trees decreases as more and more trees are added. Generally, RF works quite well with default values of hyper-parameters, and, according to these authors, typical default values for the number of trees for RF are 500 and 1000. Therefore, we chose to use 500 trees in the RF classification algorithm that was applied to the image composite classifications in this study as this number of trees has been widely used in the literature in various fields and mainly in land cover classification with very good results [60,66–70].

The image classifications for this study were based on seven main land cover classes (Table 3). The definition of these classes was based on the Yangambi land classification system [34] appropriate to the West African context which was used during the 2016 National Forest Inventory (IFN) [71]. However, to take into account the limited capacity of available images to discriminate between different land cover, some classes have been aggregated into other larger classes.

Table 3. Description of LULC categories used in the classification.

LULC Categories	Description
Dense dry forest	Dense semi-deciduous forests, plantations, gallery forests, and agroforests
Open forest	Forests with open canopies and wooded savannahs
Savannahs	Tree savannahs, shrubby savannahs, and grassy savannahs
Crop and fallow	Areas with crops and abandoned agricultural land
Buildings and bare land	Infrastructure related to human settlements and commercial centers, roads, burnt or turned soil, and mining quarry
Water bodies	Continental water surfaces (lake, lagoon, water, dam, and river)
Clouds	Surface covered by clouds and their shadows

The original spectral bands B1, B2, B3, B4, B5, and B7 from Landsat 5 and 7, together with B2, B3, B4, B5, B6, and B8 from Landsat 8, were used as inputs to the RF model for the first classification. For the second classification, an ensemble combining these same bands with the four aforementioned vegetation indices was used as input, but with the same training and validation samples.

Based upon random selection in the model, 70% of the collected data were used as training samples when classifying the composite images, while 30% were used as validation data for the classification results. The accuracy of the classifications that were performed on each image composite was then evaluated. For each image composite, we calculated traditional metrics for evaluating the accuracy of image classification, which are the producer accuracy (PA), the user accuracy (UA), the overall accuracy (OA), and Cohen's kappa coefficient (***K***) [72].

The different metrics are defined by the following equations [73]:

$$OA = (1/N) \sum_{i=1}^{r} n_{ii} \tag{1}$$

$$PA = n_{ii} / n_{icol} \tag{2}$$

$$UA = n_{ii} / n_{irow} \tag{3}$$

$$K = N \sum_{i=1}^{r} n_{ii} - \sum_{i=1}^{r} (n_{icol}\, n_{irow} / N^2) - \sum_{i=1}^{r} n_{icol}\, n_{irow} \tag{4}$$

where n_{ii} is the number of correctly classified pixels in a category; N is the total number of pixels in the confusion matrix; r is the number of classes; n_{icol} is the column total (reference data); and n_{irow} is the row total (predicted classes).

Ref. [74] defines the main parameters of classification accuracies, such as OA, as the ratio of the number of correctly classified pixels to the total number of pixels in the class, and Kappa, which refers to the proportion of error reduction between the considered classification and a completely random classification. According to [73], OA represents the ground truth classes that are correctly classified by the analyst (error of omission), while UA is the percentage of pixels that do not really belong to the reference class but are engaged in other ground truth classes (error of commission).

Following these evaluations of the classification accuracies of the image composites, the results were exported from the GEE for formatting in mapping software. The land-cover maps were finalized in ArcMap 10.6.1, while land-cover conversion maps were produced using the semi-automatic classification extension that was recently developed with python code by [75], and which is usable in QGIS 3.6. The annual rate of forest cover change (r) and annual deforestation (R), which have been defined by [76], were also calculated for the periods between the selected target years of this study and between 1985 and 2020 by applying Equations (5) and (6), as follows:

$$\mathrm{r} = \left(\frac{1}{(t_2 - t_1)}\right) * ln\left(\frac{A_2}{A_1}\right) * 100 \quad (5)$$

$$\mathrm{R} = \frac{A_2 - A_1}{t_2 - t_1} \quad (6)$$

where t_1 is year 1, t_2 is year 2, A_1 is forest area in year 1, and A_2 is forest area in year 2.

4. Results

4.1. Assessing the Accuracy of Image Classifications

Seven land cover classes were generated in a supervised manner. Using the RF algorithm in the GEE, the accuracy of the results was evaluated when vegetation indices were not used (Table 4) and when indices were used (Table 5). Overall accuracies for image composites with and without vegetation indices range from 0.91 to 0.98, while Kappa ranges from 0.86 to 0.96.

Table 4. Accuracies obtained when classifications were made without vegetation indices (PA = Producer accuracy, UA = user accuracy, OA = overall accuracy, and K = Kappa coefficient).

Image Composite	Accuracy	Clouds	Water	Dense Dry Forest	Open Forest	Crops + Fallow	Savannah	Bldg. + Soil	OA	K
1985	UA	0.94	1.00	0.95	0.85	0.94	0.98	0.93	0.95	0.93
	PA	0.99	1.00	0.95	0.75	0.97	0.97	0.89		
1990	UA	1.00	0.99	0.94	0.95	0.92	0.93	0.99	0.96	0.95
	PA	1.00	0.99	0.95	0.95	0.95	0.97	0.92		
2000	UA	0.94	0.96	0.95	0.97	0.95	0.94	0.97	0.96	0.95
	PA	0.97	1.00	0.95	0.94	0.96	0.96	0.92		
2005	UA	0.78	0.99	0.50	0.81	0.83	0.97	0.84	0.91	0.86
	PA	0.77	1.00	0.95	0.83	0.87	0.92	0.73		
2015	UA		1.00	0.95	0.65	0.90	0.95	0.97	0.98	0.96
	PA		1.00	0.98	0.83	0.93	0.90	0.95		
2020	UA		1.00	0.96	0.29	0.89	0.90	0.98	0.93	0.91
	PA		1.00	0.99	0.58	0.87	0.89	0.91		

Table 5. Accuracies obtained when classifications were made with vegetation indices (PA = Producer accuracy, UA = user accuracy, OA = overall accuracy, and K = Kappa coefficient).

Image Compos-ite	Accuracy	Clouds	Water	Dense Dry Forest	Open Forest	Crops + Fallow	Savannah	Bldg. + Soil	OA	K
1985	UA	0.92	1.00	1.00	0.84	0.95	0.97	0.91	0.94	0.93
	PA	0.99	1.00	0.97	0.76	0.96	0.96	0.89		
1990	UA	0.99	0.99	0.95	0.95	0.92	0.93	0.98	0.96	0.95
	PA	1.00	0.99	0.95	0.85	0.95	0.96	0.93		
2000	UA	0.94	0.97	0.95	0.97	0.95	0.94	0.96	0.96	0.95
	PA	0.96	1.00	0.97	0.95	0.95	0.96	0.92		
2005	UA	0.78	0.99	0.52	0.82	0.83	0.97	0.84	0.91	0.86
	PA	0.75	1.00	0.98	0.82	0.87	0.93	0,73		
2015	UA		1.00	0.97	0.62	0.90	0.97	0.96	0.98	0.96
	PA		1.00	0.98	0.79	0.92	0.90	0.96		
2020	UA		1.00	0.95	0.25	0.90	0.91	0.98	0.93	0.91
	PA		1.00	1.00	0.50	0.88	0,89	0.93		

After extracting these precision parameters from the confusion matrices of the composite classification of each target year, one of the target years (1985) without vegetation indices was presented as an example (Table A1) in Appendix A. Overall accuracies and Kappa coefficients for the classification of composite images with the original bands was very similar to those of composites made with the original bands and vegetation indices. Nevertheless, under the null hypothesis that their slopes do not differ from a 1:1 relationship, linear regressions between the values of these two types of data yield p-values much less than 0.001 for the OAs and Ks. This indicates that these values for the original band classifications of the image composites are significantly different from those including the vegetation indices. In Appendix B, this same finding of a significant difference was verified between the UA and PA accuracies for all land cover classes in all image composites (Table A2).

4.2. Distribution of Land Cover

Classifications made on the basis of the different land-cover classes that were identified made it possible to produce a land-cover map of the entire study area for each of the composite images, i.e., 1985, 1990, 2000, 2005, 2015, and 2020. The results of classifications without vegetation indices for the six targeted years were mapped (Figure 3). Regarding the results of the classifications with vegetation indices, predictions of the water body class and those of the built-up and bare land (building + soil) class were overestimated. With regard to the visual interpretation of the image composites before classification and the land cover contained in the field data, it was noted that these results of classifications with vegetation indices were not improved compared to the others and reflected the field realities less. Therefore, we decided to continue the other analyses with only those classifications without vegetation indices, considering that further, more specific studies involving the combination of other data could better elucidate the real impacts of these indices on the image classifications.

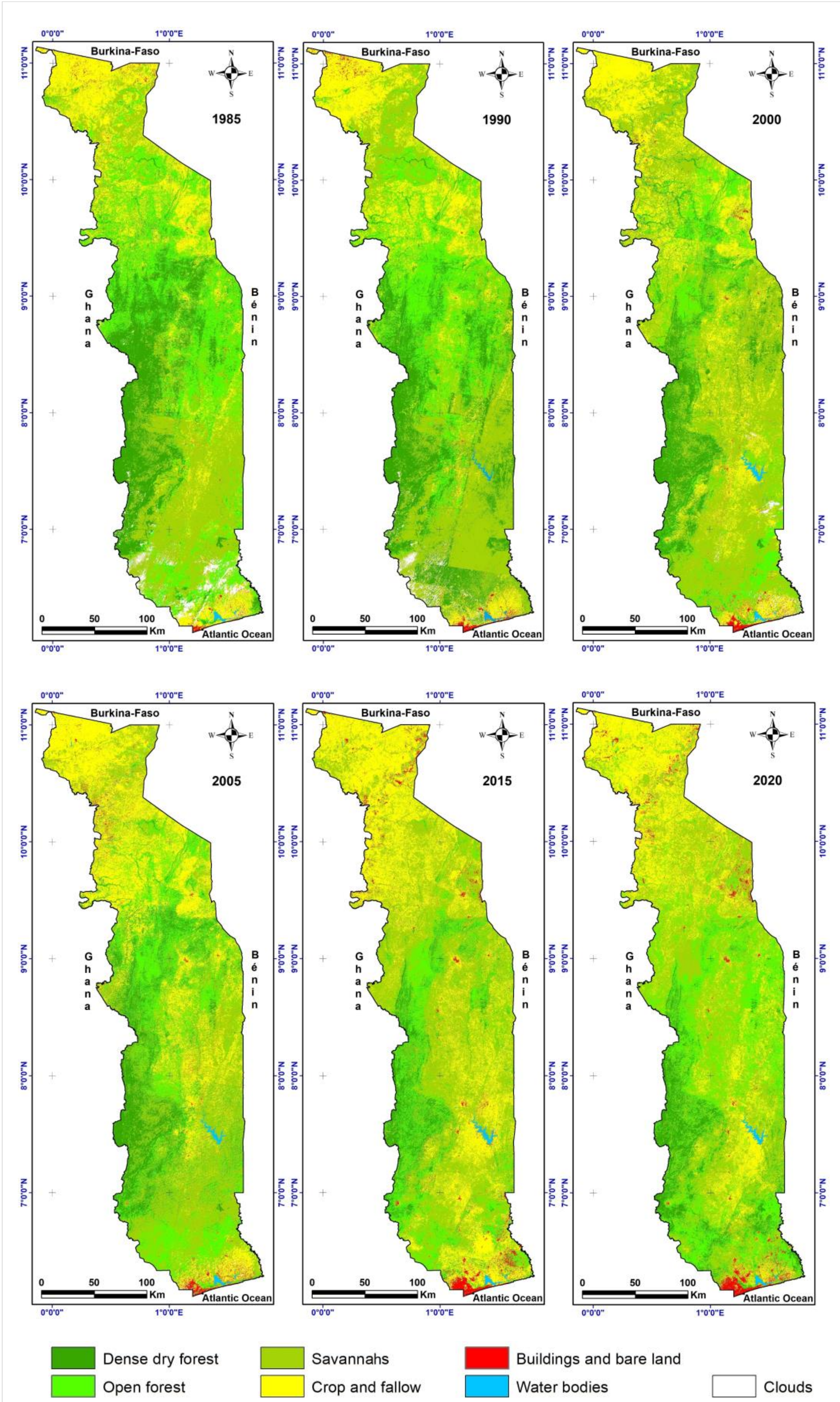

Figure 3. Land cover maps of the classifications of the six composites without vegetation indices.

Since the study area is located in tropical regions where the availability of optical data is very often limited by cloud cover [77], we included this latter as a land-cover class (but which is not presented in the following analyses). Apart from clouds, results of the classifications indicate that in 1985, there were four main land-cover classes, viz., dense dry forest (10,722.53 km^2), open forest (17,547.75 km^2), crops and fallow land (11,940.55 km^2), and savannah (14,533.13 km^2), which represented 18.92%, 30.97%, 21.07%, and 25.65%, respectively, of the nation's land surface. The lowest land-cover percentages were water bodies (0.09%) and built-up and bare soil (0.50%) classes. A quantitative evaluation of these land-cover changes and conversions between target years, as well as those between starting and ending years, was provided (Table 6).

Table 6. Land-cover change and conversions between the target years 1985-2020.

Year	LULC	Clouds	Water	Dense Dry Forest	Open Forest	Crops + Fallows	Savannah	Bldg. + Soil	Total
1985	Sup. (km^2)	1592.42	50.73	10,722.53	17,547.75	11,940.55	14,533.13	281.79	56,668.90
	Sup. (%)	2.81	0.09	18.92	30.97	21.07	25.65	0.50	100.00
1990	Sup. (km^2)	1029.65	163.44	9095.25	14,378.62	11,641.92	20,012.41	347.62	56,668.90
	Sup. (%)	1.82	0.29	16.05	25.37	20.54	35.31	0,61	100.00
	Conv. (km^2)	−562.77	112.70	−1627.27	−3169.13	−298.63	5479.28	65.83	
	Conv. (%)	−35.30	222.10	-15.20	−18.10	−2.50	37.70	23.40	
2000	Sup. (km^2)	211.48	256.37	7704.97	10,515.96	14,179.42	23,379.66	421.06	56,668.90
	Sup. (%)	0.37	0.45	13.60	18.56	25.02	41.26	0.74	100.00
	Conv. (km^2)	−818.17	92.94	−1390.29	−3862.67	2537.50	3367.25	73.44	
	Conv. (%)	−79.50	56.90	−15.30	−26.90	21.80	16.80	21.10	
2005	Sup. (km^2)	176.23	332.72	8505.64	10,439.68	19,577.14	16,956.20	681.29	56,668.90
	Sup. (%)	0.31	0.59	15.01	18.42	34.55	29.92	1.20	100.00
	Conv. (km^2)	−35.25	76.35	800.67	−76.27	5397.73	−6423.46	260.23	
	Conv. (%)	−16.70	29.8	10.40	−0.70	38.10	−27.50	61.80	
2015	Sup. (km^2)	0.00	196.67	4186.70	8549.65	20,522.50	22,045.29	1168.10	56,668.90
	Sup. (%)	0.00	0.35	7.39	15.09	36.21	38.90	2.06	100.00
	Conv. (km^2)	−176.23	−136.05	−4318.94	−1890.04	945.36	5089.09	486.81	
	Conv. (%)	−100.00	−40.90	−50.80	−18.10	4.80	30.00	71.50	
2020	Sup. (km^2)	0.00	192.02	3785.27	9709.70	21,677.56	20,146.17	1158.19	56,668.90
	Sup. (%)	0.00	0.34	6.68	17.13	38.25	35.55	2.04	100.00
	Conv. (km^2)	0.00	−4.66	−401.43	1160.05	1155.06	−1899.12	−9.91	
	Conv. (%)	0.00	−2.37	−9.59	13.57	5.63	−8.61	−0.85	
1985–2020	Sup. (km^2)	0.00	192.02	3785.27	9709.70	21,677.56	20,146.17	1158.19	56,668.90
	Sup. (%)	0.00	0.34	6.68	17.13	38.25	35.55	2.04	100.00
	Conv. (km^2)	−1592.42	141.28	−6937.26	−7838.06	9737.01	5613.04	876.40	
	Conv. (%)	−100.00	278.47	−64.70	−44.67	81.55	38.62	311.01	

Note: LULC = Land Use and Land Cover; Conv. = Conversions; Sup. = Area (Superficie); Bldg. + soil = buildings and bare land.

The area of each land cover has changed slightly for some and greatly for others in different directions in all the target years during the period considered by this study (Figure 4).

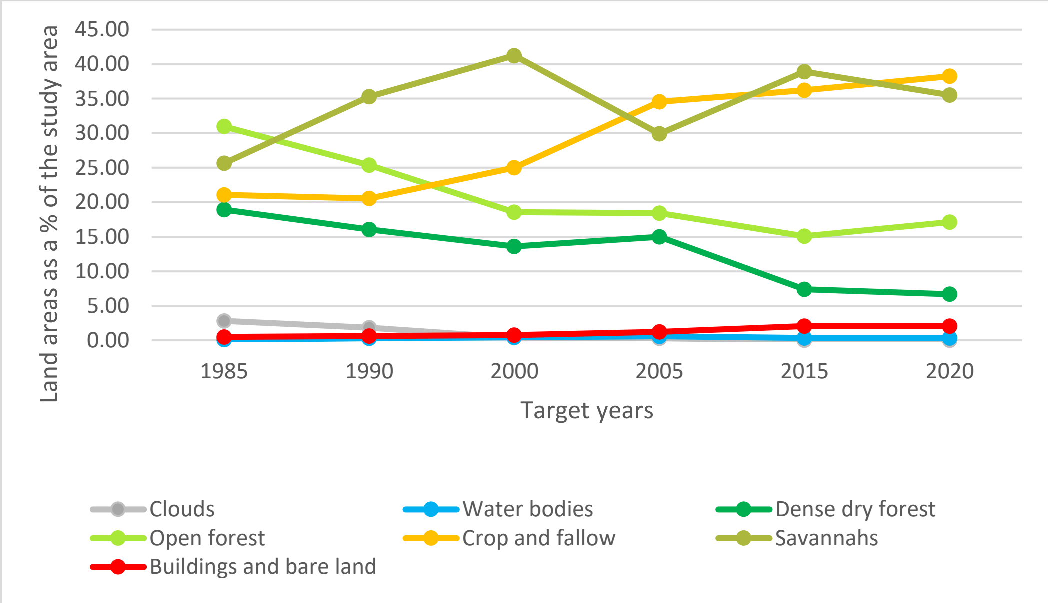

Figure 4. LULC changes as percentages of the study area.

4.3. Land-Cover Conversions

From the outset, areas of dense dry forest and open forest have decreased from 10,722.53 km^2 and 17,547.75 km^2 to 7704.97 km^2 and 10,515.96 km^2, respectively, between 1985 and 2000. During the same period, areas of crops/fallow and savannah have increased from 11,940.55 km^2 and 14,533.13 km^2 to 14,179.42 km^2 and 23,379.66 km^2, respectively. Thus, we note a 3017.56 km^2 contraction for dry dense forests and 7031.80 km^2 of open forests, while crops/fallow lands expanded by 2238.86 km^2 and savannahs by 8846.53 km^2. In 2020, these main classes occupied only 3785.27 km^2 for dense dry forests and 9709.70 km^2 for open forests, but 21,677.56 km^2 for crops/fallows and 20,146.17 km^2 for savannahs. These classes represent 6.68%, 17.13%, 38.25%, and 35.55%, respectively, of Togo's land surface area.

These changes correspond to a reduction of 64.70% of dense dry forests and 44.67% of open forests, versus an 81.55% increase in crops/fallows and 38.62% in savannahs compared to their respective starting areas. The water body area increased considerably between 1985 and 1990, through the construction of a large hydroelectric dam at Nangbeto in the southeastern part of the country (1987), together with the creation of other small water reservoirs. Built-up (buildings) and bare land (bare soil) class areas increased by +300%, from 281.79 km^2 in 1985 to 876.40 km^2 in 2020. In short, all land cover has changed during the period covered by the study, with a decrease in areas of dense dry forest and open forest, accompanied by a sharp increase in the areas of crops/fallow lands and savannahs. For illustrative purposes, the conversions from one land cover to another, as well as areas that were retained and not changed during the 2015 to 2020 period, are shown in Figure 5. The same types of charts for other time periods (1985 to 1990, 1990 to 2000, and 2000 to 2005) are provided (Figures A1–A3) in Appendix C.

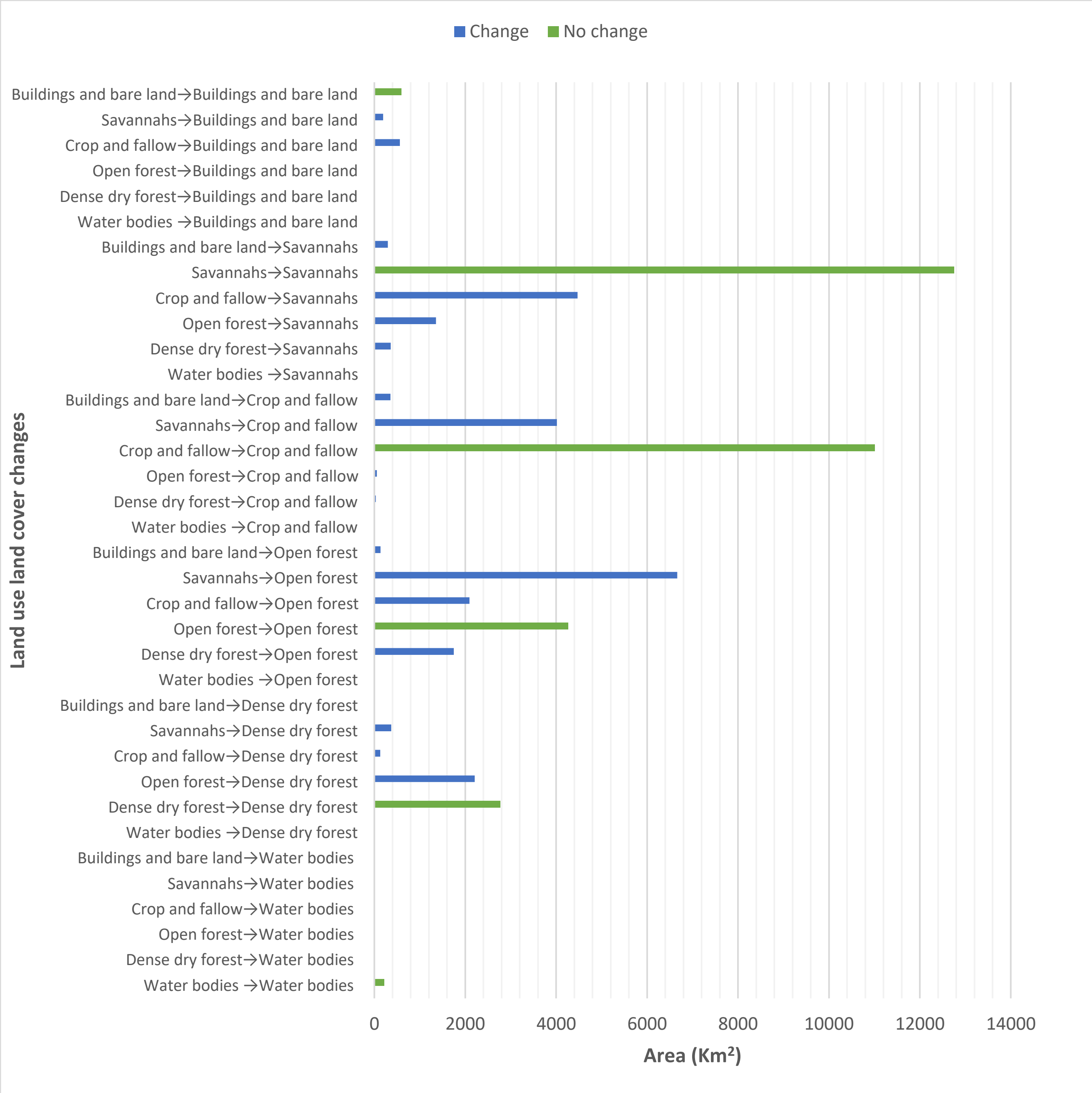

Figure 5. Land-cover conversions that occurred between 2015 and 2020.

Maps of the changes were then produced (Figure 6) by combining all classes that had undergone conversions on one hand, and all those that had not undergone conversion during the periods that were considered on the other. The change map between the 2005 and 2015 classifications was not produced because images of the first four target years have one more land-cover class (i.e., clouds) than the last two. Therefore, the application of the change detection algorithm between these two years (with a different number of land-cover classes) generates several hybrid classes that do not reflect the situation on the ground.

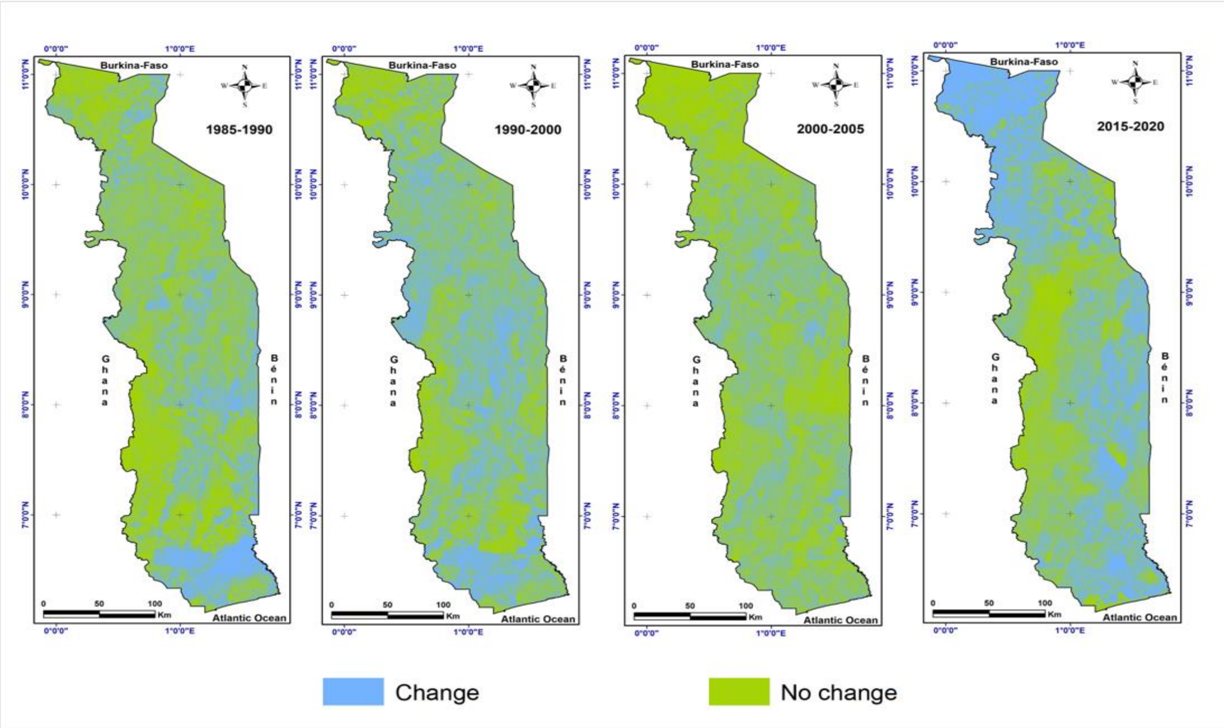

Figure 6. LULC change maps.

4.4. Evolution of Forest Cover

When considering only dense dry forest and open forest classes, their respective starting areas were 10,722.53 km^2 and 17,547.75 km^2 in 1985, i.e., 18.92% and 30.97% of the nation's total territory. Under the effects of land-cover change, they have decreased to 16.05% and 25.37% in 1990, 13.60% and 18.56% in 2000, 15.01% and 18.42% in 2005, 7.39% and 15.09% in 2015, and to 6.68% and 17.13% in 2020. With an area of 3785.27 km^2 for dense dry forests and 9709.70 km^2 for open forests in 2020, forest areas have thus declined by 12.24% for the first category and 13.83% for the second, i.e., a total of 26.07% at the national level during the 35 years covered by this study. Details on the quantification of these two land covers in the different ecological zones and their changes over time are indicated in Appendix D (Table A3).

To facilitate the subsequent quantitative analysis of forest cover change, we have cumulated the two aforementioned occupancy classes to form the forest class. The trend line (Figure 7) that summarizes the percentage change in forest area relative to that of the country illustrates the degree of deforestation and forest degradation over the period that was considered. Forest area distributions as a land-cover percentage by ecological zone and by target year were estimated (Figure 8).

When we explored the data at the level of ecological zones to determine how these forest areas have changed through time, we noted that the deforestation or degradation of these forests has not proceeded at the same rate in these ecosystems. The evolutions of forest areas in the different ecological zones were illustrated by the distribution maps of forest cover of the target years from the period from 1985 to 2020 (Figure 9).

In ecological zones I, II, and III, these forested areas declined almost continuously from 1985 with a cumulative loss until 2020 of 16.73%, 48.62%, and 28.66%, respectively, compared to their starting size in these areas. We can, nevertheless, note a forest area recovery in the 2015 to 2020 period in zone I and between 2000 and 2005 in zone II. Zone IV (the smallest ecological zone) experienced a sharp decline in forest area (18.35%) between 1985 and 1990, followed by a smaller loss (7.41%) between 1990 and 2000, prior to its recovery and then contraction (to 1.58%) from 2015 to 2020. Zone V is characterized by a 30.49% loss of forest area between 1985 and 1990, then a rapid increase in area (21.73%)

for a decade (1990–2000). These areas continued to increase until 2005 and then declined slightly from 2005 to 2015 before increasing again to 29.2% of the total area in 2020.

The finer-scale examination (zooming) of the maps produced from the results (Figure A4) in Appendix E shows the development of two towns (Sokodé and Tchamba), as well as the Abdoulaye Forest Reserve between 1985 and 2020. We noted the expansion over time of both these towns and agriculture, as well as the appearance of small new settlements at the expense of wooded areas. As a result of these two main factors, the average annual rate of change of forest cover to other land cover is about −2.11% between 1985 and 2020, leading to the disappearance of more than half of the forest areas during this period.

The results of calculating the annual rate of change in forest cover and annual deforestation between individual target years, and from the beginning to the end of the study period are shown (Table 7).

4.5. Land-Cover Changes at the Administrative Regions Scale

Following the analysis of land-cover conversions at the national level and the evolution of forest cover in the ecological zones, the quantification of all changes that have occurred at the level of the administrative regions was mapped (Figure 10).

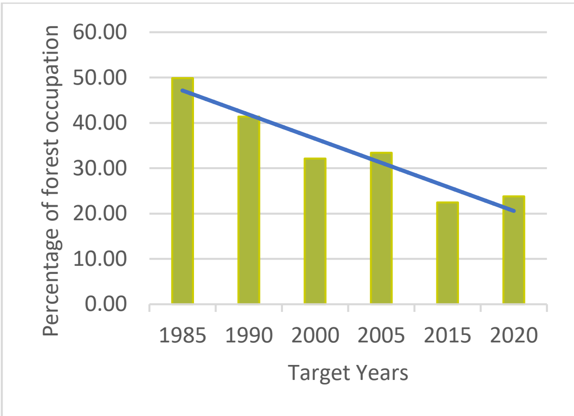

Figure 7. Countrywide forest percentage changes.

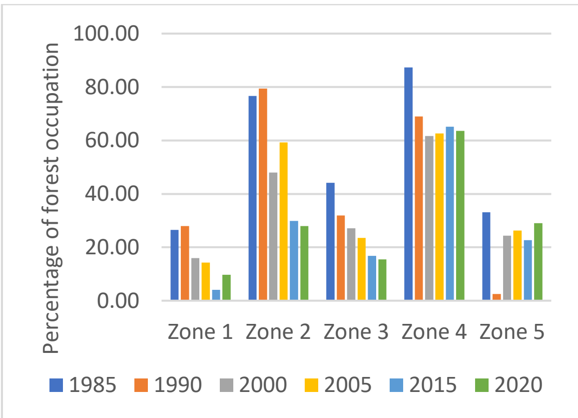

Figure 8. Forest change by ecological zone.

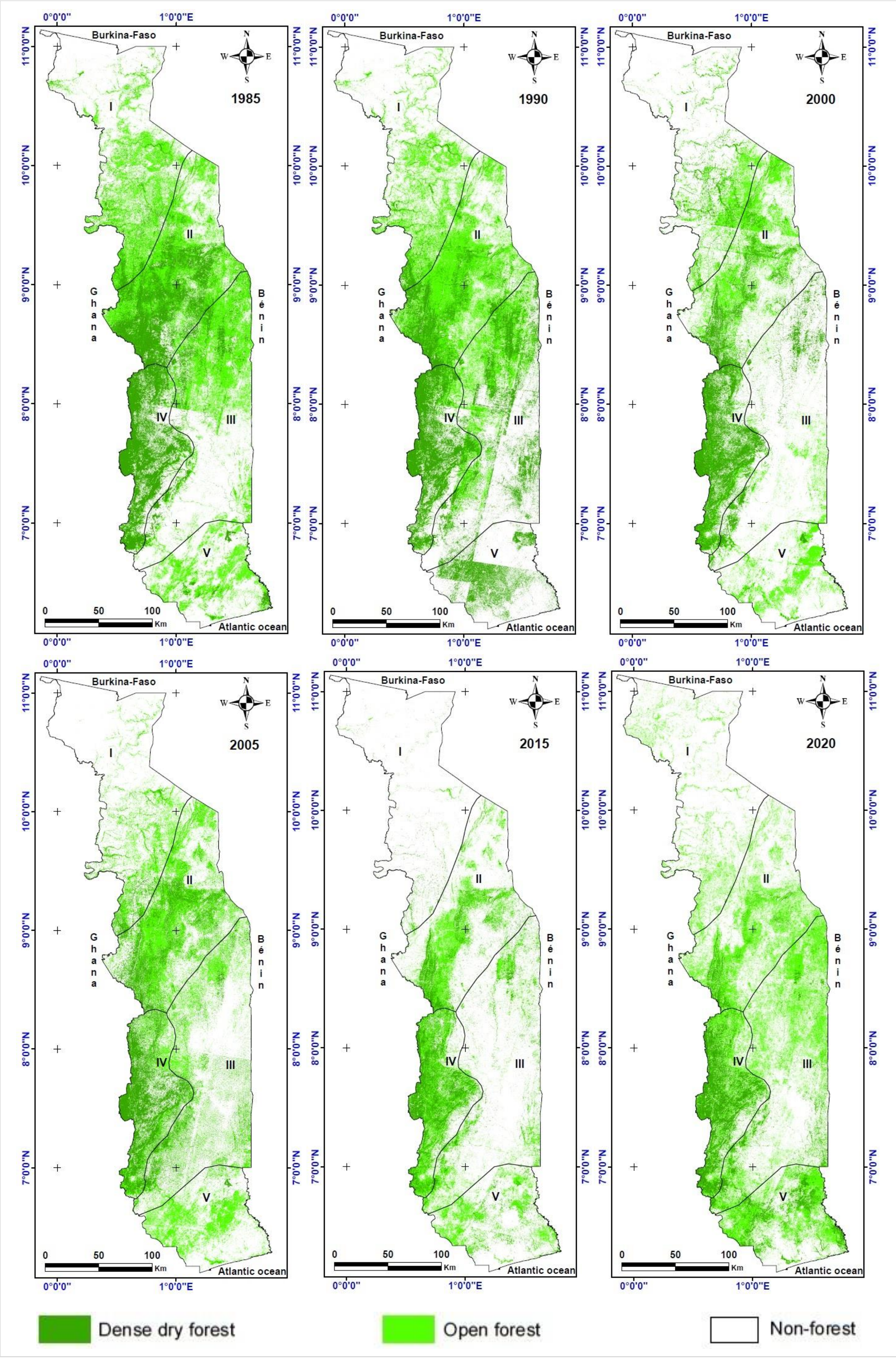

Figure 9. Forest evolution across ecological zones by target year.

Table 7. Evolution of forested areas between 1985 and 2020.

Year	Area (km^2)	Forest Area (% of Togo)	r (% y^{-1})	R (km^2 y^{-1})
1985	28,270.28	49.89		
1990	23,473.88	41.42	−3.72	959.28
2000	18,220.92	32.15	−2.53	525.30
2005	18,945.32	33.43	0.78	−144.88
2015	12,736.35	22.48	−3.97	620.90
2020	13,494.97	23.81	1.16	−151.72
1985–2020			−2.11	422.15

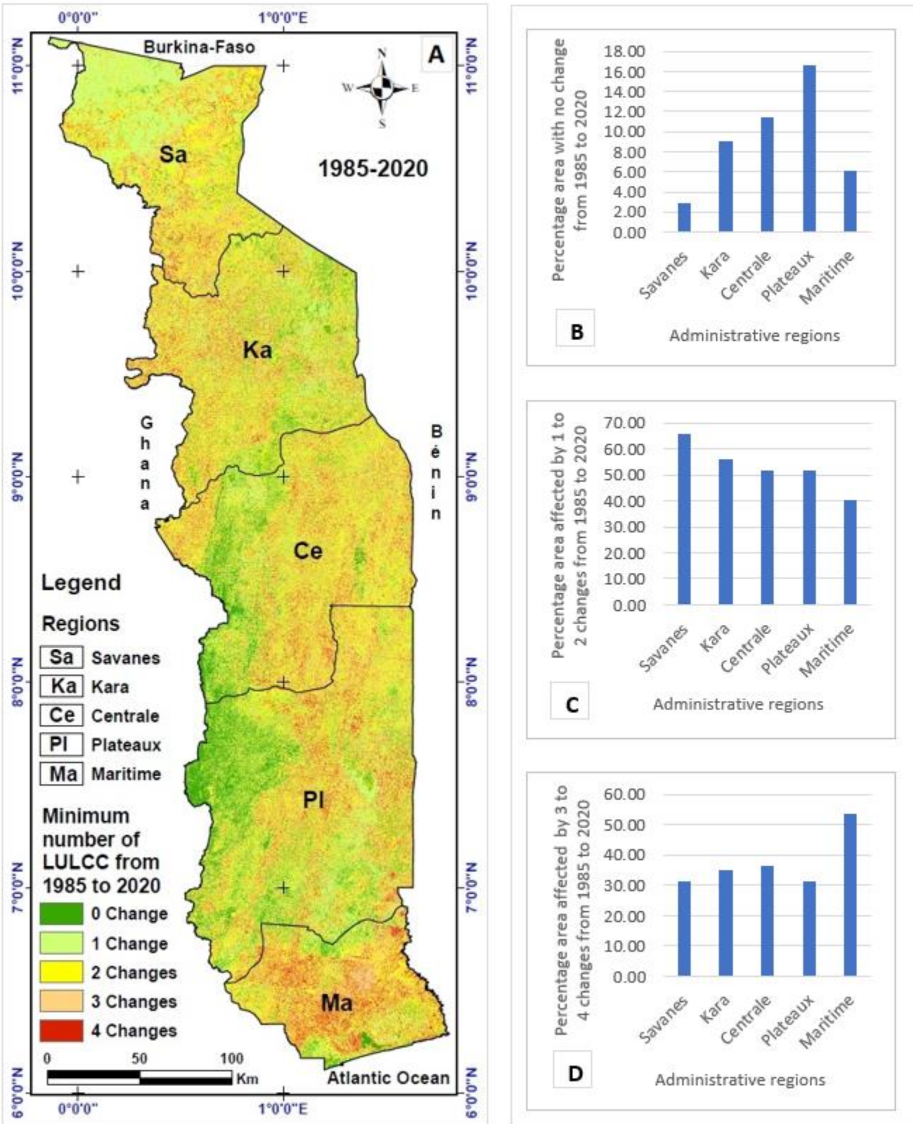

Figure 10. (**A**) Land-cover change gradient by region from 1985 to 2020; (**B**) area unchanged; (**C**) area with one to two changes; and (**D**) area with three to four changes.

In all of these administrative regions, original land covers were retained in part during the period covered by the study (Figure 10A). For those remaining parts where the land cover was altered, they had undergone at least one, two, three, or four changes between

1985 and 2020. Visual inspection reveals that parts where little or no change had been experienced were mostly forested areas (e.g., from the northeast to southwest), urban areas such as the national capital Lomé, and large bodies of water such as Lake Togo in the extreme south of the country. The Plateaux administrative region retained the most area (16.69%) of this land cover that had never changed (Figure 10B). This region is followed by the Centrale (11.48%), Kara (9.09%), and Maritime (6.12%) regions, while the Savanes region has the smallest proportion (2.84%) of its area not being affected by change over the 35-year period.

It can be observed that 65.75% of the Savanes region has undergone at least one to two changes in land cover (Figure 10C). In the Kara, Centrale, and Plateaux regions, slightly more than half of their respective areas have been similarly affected. In contrast to the areas by region that have never undergone change, the Maritime region has the largest percentage of the regional area (53.50%) that has undergone at least three to four land-cover changes (Figure 10D). For the same locations, land-cover changes have occurred more rapidly in the Maritime, followed by the Centrale (36.59%), Kara (34.98%), (31.44%), and Savanes (31.41%) regions.

5. Discussion

5.1. Quality of Results from Composite Image Classifications

During this study, data from Landsat 5, 7, and 8 archives were used to form different image composites, the supervised classifications of which (under the GEE platform) led to the production of land cover maps of Togo. Despite difficulties that were encountered in finding the best quality images, the results that were obtained indicate relatively high overall accuracies of 91% to 98% for composites with the original bands and 86% to 96% for those including the vegetation indices. However, the classification results including vegetation indices tended to overestimate the built-up and bare land (buildings + soil) class and the water body class. We believe that this is likely due to the simultaneous presence of NDBI, which captures residential areas and bare soil, the BSI, which is a bare soil-specific index, and NDWI, which would have difficulty distinguishing water bodies from shadows. These results are consistent with those of [78] and [24], who found that the NDBI and modified NDWI yielded image classification results with very low accuracies, despite being two popular indices in the literature.

The results have shown that OA and *K*s for the original composite band classifications are significantly different from those with vegetation indices, but the latter did not improve the image classification results as one would have expected. Nevertheless, the spontaneous decrease in overall accuracy and *K*s for the 2005 composite classification (Tables 4 and 5) could be primarily related to deficiencies in the Landsat 7 data that are observed as fine stripes on the 2005 map (Figure 9). It should be noted that this sensor suffered hardware failure in its Scan Line Corrector (SLC) in 2003, resulting in the loss of about 22–25% of the data in each scene [79]. Additional research could be done on the impact of these indices on the quality of image classification results and also test new indices such as the Emissivity Contrast Index (ECI), which have overcome the NDVI limitation concerning its capability to distinguish bare soil from senescent vegetation [80]. Another thing that could be tested in future research using RF in order to improve image classification accuracy is to tune the hyper-parameters of this model to improve its performance [65], instead of using the default number of trees.

5.2. Land-Cover Changes

The classifications indicate fairly rapid changes in land cover over the 35 years that are covered by this study and the rapid deforestation or degradation of forest cover, the area of which fell countrywide from 49.89% in 1985 to 23.81% in 2020. These changes have favored crops and fallow lands, savannahs, urban areas, and bare soil. In considering the evolution of forest areas in the different ecological zones, we found that zones II and IV, which cover 32.55% of the national area, contained 55.10% of the national forest cover in

2020. This could be explained by the fact that these two zones are mountainous with very steep relief (Figure 1B), making it very difficult to access forest resources and land in these zones. Zone IV, in particular, has retained most of its original forest area (72.77%), even though it is the smallest of the five ecological zones. Furthermore, ecological zones I and III are areas par excellence in terms of agriculture and housing, as can be seen in our mapped results. Zone V is home to more than one-third of the country's population; the relatively broad extent of forest that was found in this zone would have more to do with poor image quality than with the actual area.

In Table 7, we note that r is negative and R is positive when there is a contraction of forested areas, while the opposite occurs when there is an expansion of forested areas. From these two indicators of forest cover change, we further note that the study area experienced a substantial loss of forest area between 1985 and 2000 and, again, between 2005 and 2015. In contrast, only small increases in the area occurred until 2005 and, again, between 2015 and 2020. Current forest area declines are most likely related to agricultural expansion and rapid human population growth in Togo (2.84% y^{-1}), which exert strong pressures on natural resources and land. The national REDD+ Togo study of 2018 on the causes and consequences of deforestation and forest degradation across the nation has confirmed that agricultural development, including associated management practices (notably, the use of fire), is the main cause of forest disturbance, ahead of timber exploitation (timber and energy) and urban expansion. Furthermore, the dynamics of urbanization, which underlies the country's population growth, are driving rapid changes in LULC and are contributing to forest loss, both directly and indirectly [32,33].

Nevertheless, the increase in forest area in 2005 could be attributed simply to the aforementioned poor quality of Landsat 7 data, which would influence the classifiers during processing. The 2020 increase could be due to an overestimation by classifiers of the open forest class at the expense of savannah, but this could also be due to the results of conservation policies and programs that have been recently implemented by the government (forest inventory and REDD + strategy). In order to achieve the state's objective of increasing forest cover to 30% of the territory by 2030, these factors of forest degradation would have to be reconsidered in terms of governmental actions at the social, environmental, and political levels. In addition, the rate of land-cover conservation and the speed of change that has been quantified at the level of administrative regions indicate that the Plateaux and Centrale regions are better conserved, while the Maritime region records the highest frequency of change. The Savanes region is intermediate between these two extremes; most land cover has only changed once or twice. Yet, it should be noted that most of the plant formations of the Savanes region were very early transformed into crops and remained in this class. This explains why this region has a relatively low rate of land cover change for a given location despite its higher rate of degraded area. The Maritime region has experienced the most land-cover changes over the period, i.e., three to four times. These conditions would thus need to be monitored when making land-cover planning or development decisions. Given that forest management across the study area is based more on administrative subdivisions, our results should enable centralized administrative and forestry authorities to prioritize actions for a much more balanced environmental governance.

5.3. Advantages and Limitations of the Method Used

For the selection, pre-processing, and classifications of satellite images during this study, we used the RF algorithm, which can take into account even disparate data to make a fairly accurate classification of heterogeneous land cover such as in forest-savannah mosaics [60]. This algorithm has been used on the GEE platform containing a vast catalog of Earth observational data. It is based upon millions of servers around the world that allow for the rapid processing and analysis of satellite data over large areas, without the need to download them [81]. The GEE has a user-friendly programming environment with high computational efficiency, which allows less time to be spent on usual satellite data processing steps that are frequently quite time-consuming when using dedicated software.

A further advantage of this method is the possibility of making enormous savings in both time and money when conducting regional or national forest inventories. For example, when considering the results that were obtained for several land-cover classes through methods requiring very few means that were applied in this study, we note that they are more or less comparable to those that were obtained from the national forest inventory (NFI), which had mobilized many more human and financial resources. For the 2015 results (the year closest to the NFI), we obtained 22.48% for the forest class, 38.90% for the savannah class, and 38.27% for the grouping of agriculture and infrastructure classes versus 24.24%, 34.86%, and 40.90, respectively, for the 2016 NFI [71]. With this method of processing satellite data in the GEE, once the processing code is completed, it can be easily optimized and applied for the long-term monitoring of LULC changes when incorporating newly acquired images [62].

However, it must be noted that this processing power is not available on demand for all types of operations, given that a quota is allocated to each user and, thus, the GEE system sometimes limits or aborts certain code executions that are computationally demanding [26]. Furthermore, despite having millions of images, some areas have long periods when cloud-free data are absent, especially in tropical environments. This is a particularly lamentable state of affairs, given that research in this region has calculated the probability of acquiring Landsat MSS or Landsat TM images with <70% cloud cover in a year to be only 26% [79]. In these cases, the GEE permits the selection of pixels from multiple images exhibiting large temporal differences in acquisition dates to form the composite, as was the case in our study. Unfortunately, such selections do not allow for estimates of seasonal differences or phenologies, thereby introducing potential classification errors. A further limitation is that during satellite data processing, code execution errors that are encountered can be difficult to debug, given that scripts in the GEE run in the Google Cloud. As confirmed by [62], errors also can occur in the JavaScript code, either on the client side, which is manageable with some effort, or during server-side execution, a situation that can be very difficult to manage.

6. Conclusions

The LULC changes that are attributable to anthropogenic disturbance are leading to reductions in forest cover, contributing significantly to global carbon emissions. In this study, we employed the median satellite image composition method with historical Landsat sensor data in the GEE to quantify changes across the nation of Togo between 1985 and 2020 using the Random Forest algorithm. Our results indicate that all land-cover classes identified from the 1985 composite image were affected to varying degrees by these land-cover changes. Furthermore, forests lost about 52.28% of their original area from 1985 to 2020 through the expansion of crop and fallow lands, savannah, and urbanization. Ecological zones I, III, and V cover more than two-thirds of the total area of the country and contain less than half of the forest cover. The changes are mainly reflected by a strong increase in agricultural activity, deforestation through timber exploitation, and the urban expansion of a burgeoning human population. Easier accessibility of the areas and a greater human presence favor all of these activities. In contrast, ecological zones II and IV, which cover less than one-third of the total area of the country, contain more than 55% of the national forest cover in 2020. These are very mountainous areas, the steep slopes of which limit the adverse effects of human activities and, consequently, their effects on natural resources.

The methods that were applied in this study and the results that were obtained could help forestry and territorial administrators to better understand the factors that are involved in land-cover change and forest area reduction. They could also help the national coordination of REDD+ in Togo to better operate or to boost the measurement, reporting, and verification system, as part of the nation's forest monitoring system. For similar future studies in Togo, more reliable satellite data (Landsat 8 and 9) with lower cloud cover or higher spatial resolution (Sentinel 2 and greater) could be used when sufficient time-series images become available on the GEE platform over the study area, as well as other countries in Sub-Saharan Africa.

Author Contributions: Conceptualization: A.K. and K.G.; Methodology: A.K., K.G. and F.F.; Data collection: A.K., F.F., W.A., M.D. and K.W.; Data analysis: A.K. and K.G., Preparation of the manuscript draft: A.K.; Supervision: K.G.; Writing and editing: all authors. All authors have read and agreed to the published version of the manuscript.

Funding: This research has been funded by the *Programme Canadien de bourses de la Francophonie* (Government of Canada, Department of Foreign Affairs, Trade and Development, Canadian Partnership Branch), as well as the *Natural Sciences and Engineering Research Council of Canada* (NSERC Discovery grant RGPIN-2018-06101 and NSERC CREATE Grant 543360-2020).

Institutional Review Board Statement: Not applicable.

Informed Consent Statement: Not applicable.

Data Availability Statement: Data are available upon request and can be obtained by contacting the lead author.

Acknowledgments: We thank all of the reviewers for their guidance and contributions to writing and commenting on this manuscript. W.F.J. Parsons translated the French text.

Conflicts of Interest: The authors declare no conflict of interest. The organization providing the funding has played no role in the design of the study, collection, analysis, interpretation of the data, writing of the manuscript, or in the decision to publish the results.

Appendix A

Table A1. Confusion matrix for the target year 1985 without vegetation indices. Perfectly predicted values for each category are highlighted in bold along the diagonal.

	Clouds	Water	Dense Dry Forest	Open Forest	Crops + Fallows	Savannah	Bldg. + Soil	Producer Accuracy
Clouds	25,986	0	0	0	0	147	0	0.99
Water	0	8805	1	0	0	14	2	1.00
Dense dry forest	0	0	129,893	3690	249	138	0	0.97
Open forest	0	0	7144	26,071	1390	138	0	0.75
Crops + fallows	171	0	167	570	123,841	893	2649	0.97
Savannah	1053	0	30	174	1715	117,812	818	0.97
Bldg. + Soil	297	0	72	111	3974	1523	46,131	0.89
User Accuracy	0.94	1.00	0.95	0.85	0.94	0.98	0.93	
Overall Accuracy					0.95			
Kappa					0.93			

Appendix B

Table A2. Comparison of accuracies by land-cover class; with vs. without vegetation indices.

Classes	Accuracy	p-Value
Water	UA	0.000
	PA	0.001
Dense dry forest	UA	0.000
	PA	0.001

Table A2. *Cont.*

Classes	Accuracy	*p*-Value
Open forest	UA	0.000
	PA	0.001
Crops + fallows	UA	0.000
	PA	0.000
Savannah	UA	0.001
	PA	0.000
Bldg. + soil	UA	0.000
	PA	0.000

Appendix C

Conversion of Land-Cover Classes

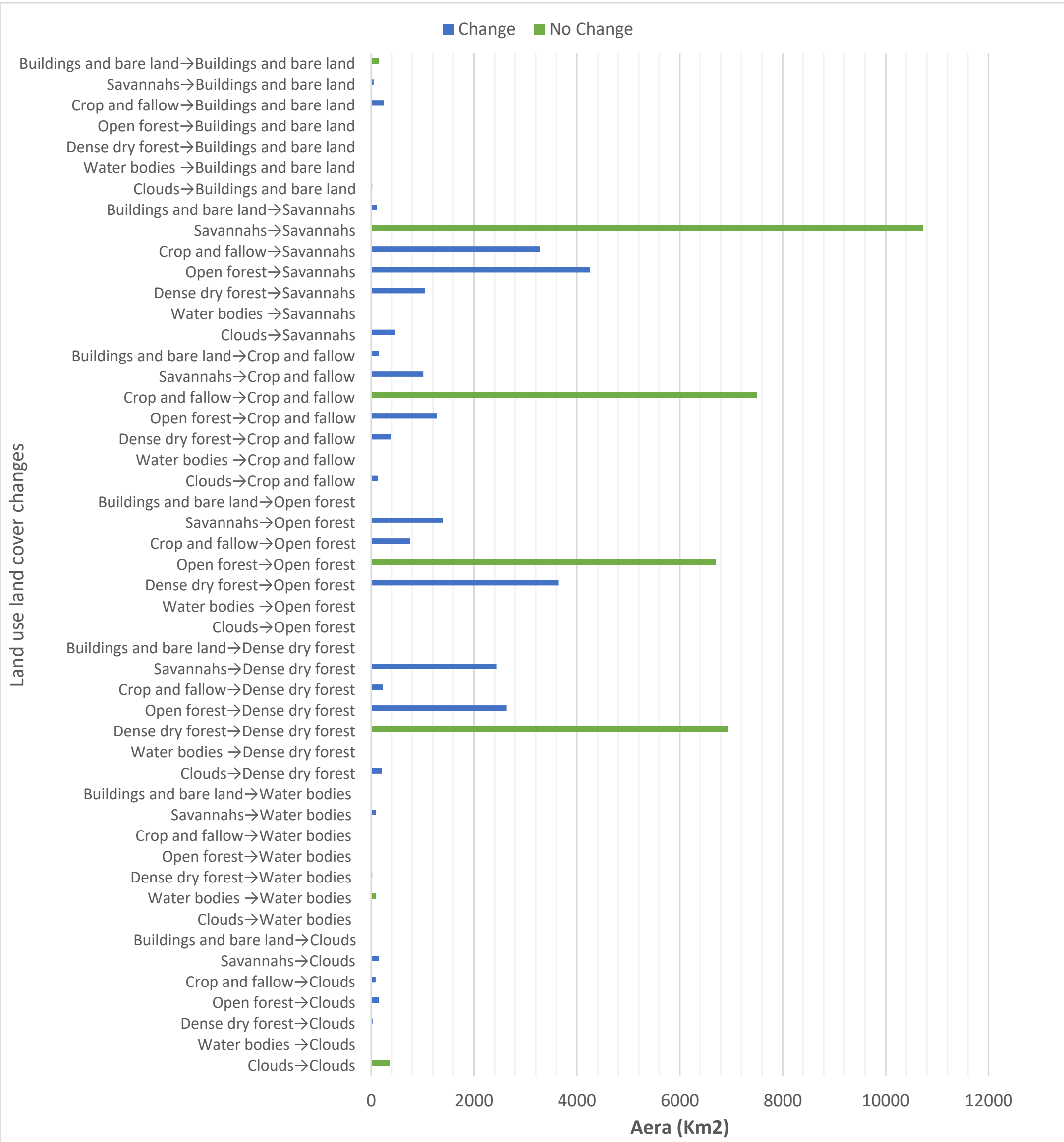

Figure A1. Land-cover conversions between 1985 and 1990.

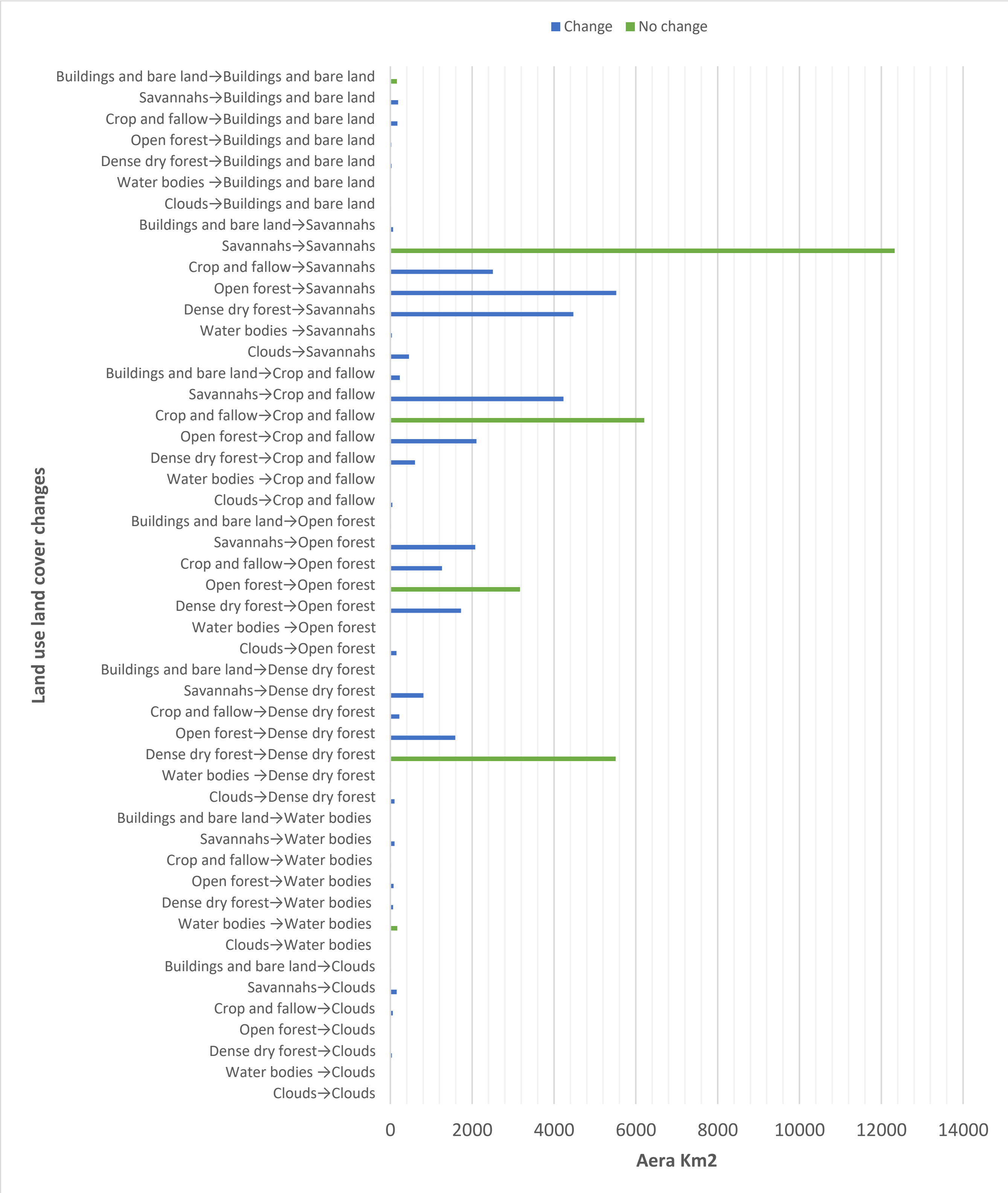

Figure A2. Land-cover conversions between 1990 and 2000.

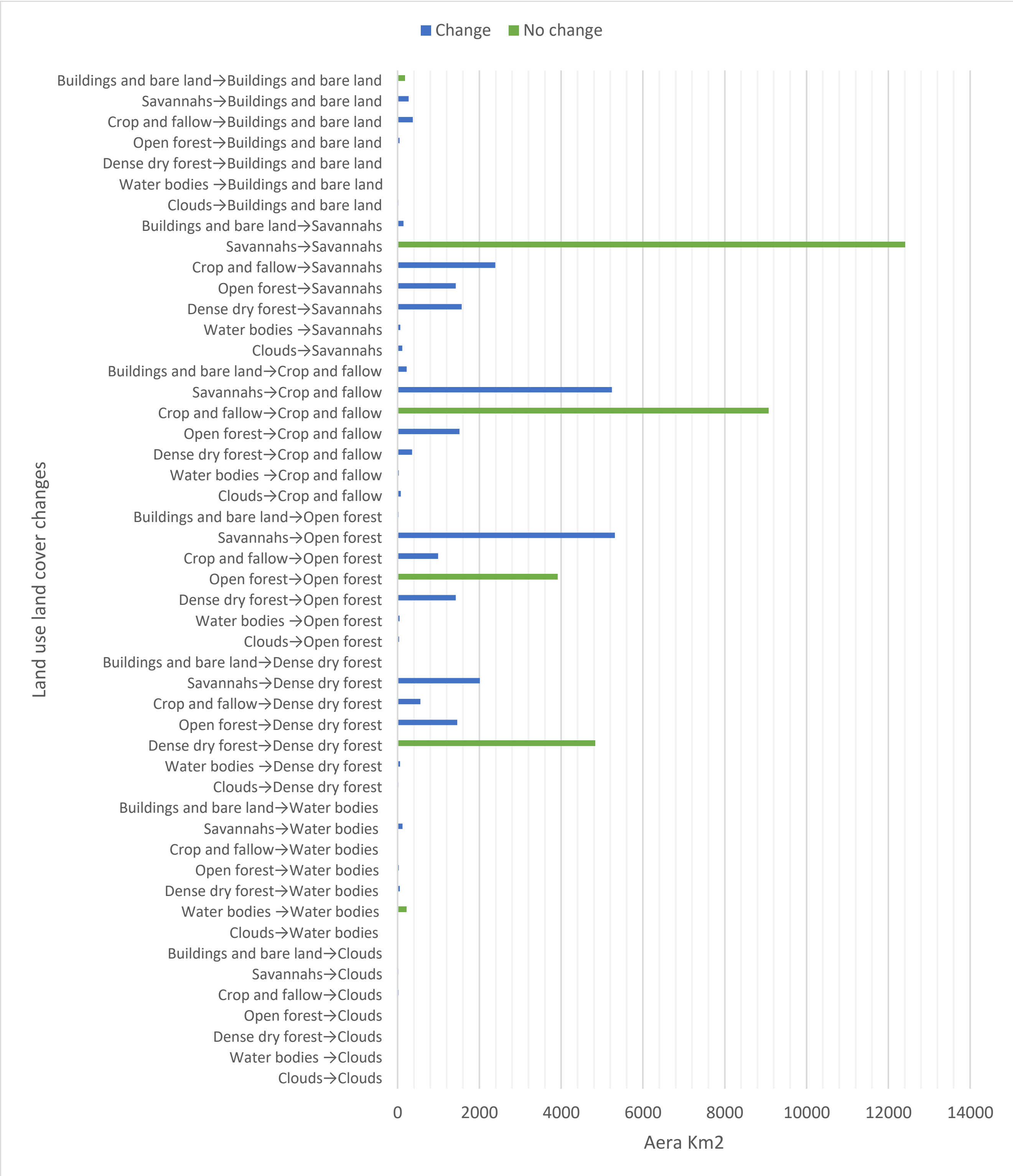

Figure A3. Land-cover conversions between 2000 and 2005.

Appendix D

Table A3. Changes in forest-covered areas.

Years	Classes	Zone I	Zone II	Zone III	Zone IV	Zone V	Total
1985	Dense dry forest	878.81	3977.56	1491.35	4192.75	182,06	10,722.53
	Open forest	3039.83	5253.77	5634.57	1392.29	2227,29	17,547.75
	Forest areas	3918.64	9231.32	7125.92	5585.04	2409.35	28,270.28
	%/Country	6.91	16.29	12.57	9.86	4.25	49.89
	%/Zone	26.47	76.60	44.17	87.37	33.07	
1990	Dense dry forest	542.65	3054.40	1562.54	3752.49	183.18	9095.25
	Open forest	3599.47	6522.88	3592.65	659.38	4.25	14,378.62
	Forest areas	4142.12	9577.28	5155.19	4411.86	187.43	23,473.88
	%/Country	7.31	16.90	9.10	7.79	0.33	41.42
	%/Zone	27.98	79.47	31.95	69.02	2.57	
2000	Dense dry forest	370.09	2463.65	1407.70	3316.65	146.87	7704.97
	Open forest	1989.39	3313.71	2967.11	621.64	1624.10	10515.96
	Forest areas	2359.48	5777.36	4374.81	3938.29	1770.98	18,220.92
	%/Country	4.16	10.19	7.72	6.95	3.13	32.15
	%/Zone	15.94	47.94	27.12	61.61	24.30	
2005	Dense dry forest	392.21	3148.15	1577.43	3228.93	158.92	8505.64
	Open forest	1714.80	3996.35	2206.50	770.48	1751.55	10,439.68
	Forest areas	2107.01	7144.50	3783.93	3999.41	1910.47	18,945.32
	%/Country	3.72	12.61	6.68	7.06	3.37	33.43
	%/Zone	14.23	59.28	23.45	62.57	26.22	
2015	Dense dry forest	145.76	1025.65	752.59	2136.58	126.13	4186.70
	Open forest	463.68	2578.21	1957.75	2028.74	1521.27	8549.65
	Forest areas	609.44	3603.86	2710.34	4165.31	1647.40	12,736.35
	%/Country	1.08	6.36	4.78	7.35	2.91	22.48
	%/Zone	4.12	29.90	16.80	65.16	22.61	
2020	Dense dry forest	128.64	975.70	365.86	2076.96	238.12	3785.27
	Open forest	1313.22	2395.81	2136.68	1987.47	1876.52	9709.70
	Forest areas	1441.85	3371.51	2502.53	4064.43	2114.63	13,494.97
	%/Country	2.54	5.95	4.42	7.17	3.73	23.81
	%/Zone	9.74	27.98	15.51	63.59	29.02	
Ecological Zone areas		14,805.30	12,051.40	16,133.60	6392.10	7286.50	56,668.90

Appendix E

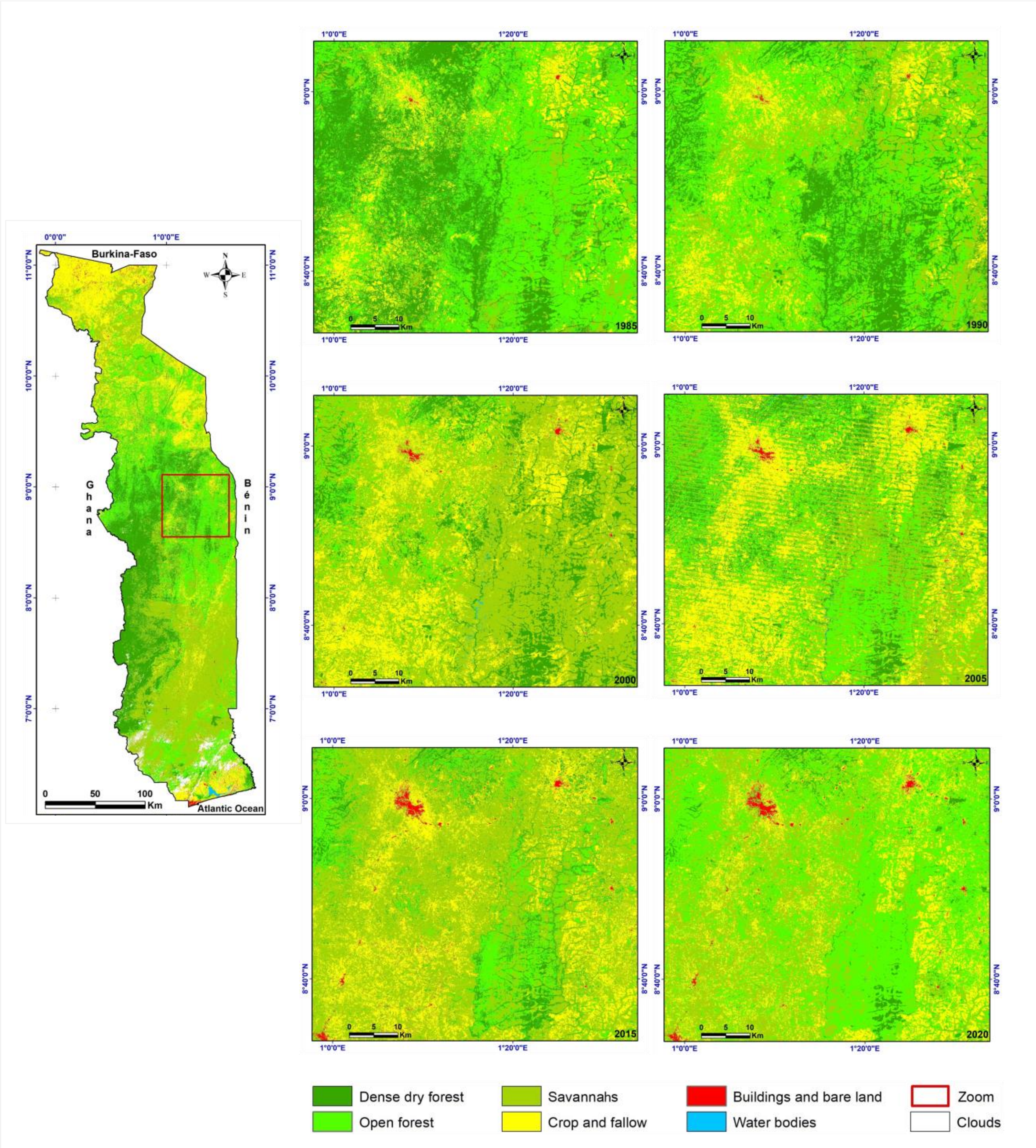

Figure A4. Enlarged ("zoomed") insets in East-Central Togo for all target years.

References

1. Nunes, L.J.R.; Meireles, C.I.R.; Pinto Gomes, C.J.; Almeida Ribeiro, N.M.C. Forest Contribution to Climate Change Mitigation: Management Oriented to Carbon Capture and Storage. *Climate* **2020**, *8*, 21. [CrossRef]
2. Cardil, A.; de-Miguel, S.; Silva, C.A.; Reich, P.B.; Calkin, D.; Brancalion, P.H.S.; Vibrans, A.C.; Gamarra, J.G.P.; Zhou, M.; Pijanowski, B.C.; et al. Recent Deforestation Drove the Spike in Amazonian Fires. *Environ. Res. Lett.* **2020**, *15*, 121003. [CrossRef]
3. Laumonier, Y.; Edin, A.; Kanninen, M.; Munandar, A.W. Landscape-Scale Variation in the Structure and Biomass of the Hill Dipterocarp Forest of Sumatra: Implications for Carbon Stock Assessments. *For. Ecol. Manag.* **2010**, *259*, 505–513. [CrossRef]

4. Gogoi, A.; Ahirwal, J.; Sahoo, U.K. Plant Biodiversity and Carbon Sequestration Potential of the Planted Forest in Brahmaputra Flood Plains. *J. Environ. Manag.* **2021**, *280*, 111671. [CrossRef]
5. Kundu, K.; Halder, P.; Mandal, J.K. Forest Cover Change Analysis in Sundarban Delta Using Remote Sensing Data and GIS. In *Intelligent Computing Paradigm: Recent Trends*; Mandal, J.K., Sinha, D., Eds.; Studies in Computational Intelligence; Springer Singapore: Singapore, 2020; pp. 85–101, ISBN 9789811373343.
6. FAO and UNEP. *The State of the World's Forests 2020: Forests, Biodiversity and People*; The State of the World's Forests (SOFO); FAO and UNEP: Rome, Italy, 2020; ISBN 978-92-5-132419-6.
7. Chen, Y.-Y.; Huang, W.; Wang, W.-H.; Juang, J.-Y.; Hong, J.-S.; Kato, T.; Luyssaert, S. Reconstructing Taiwan's Land Cover Changes between 1904 and 2015 from Historical Maps and Satellite Images. *Sci. Rep.* **2019**, *9*, 12. [CrossRef]
8. Deo, R.K.; Russell, M.B.; Domke, G.M.; Andersen, H.-E.; Cohen, W.B.; Woodall, C.W. Evaluating Site-Specific and Generic Spatial Models of Aboveground Forest Biomass Based on Landsat Time-Series and LiDAR Strip Samples in the Eastern USA. *Remote Sens.* **2017**, *9*, 598. [CrossRef]
9. Olorunfemi, I.E.; Olufayo, A.A.; Fasinmirin, J.T.; Komolafe, A.A. Dynamics of Land Use Land Cover and Its Impact on Carbon Stocks in Sub-Saharan Africa: An Overview. *Environ. Dev. Sustain.* **2021**, *24*, 40–76. [CrossRef]
10. Angelsen, A.; Brockhaus, M.; Sunderlin, W.D.; Verchot, L.V. *Analyse de la REDD+ Les Enjeux et les Choix*; CIFOR: India Nishiya, Momono, 2013; ISBN 978-602-1504-00-0.
11. Minh, D.H.T.; Ndikumana, E.; Vieilledent, G.; McKey, D.; Baghdadi, N. Potential Value of Combining ALOS PALSAR and Landsat-Derived Tree Cover Data for Forest Biomass Retrieval in Madagascar. *Remote Sens. Environ.* **2018**, *213*, 206–214. [CrossRef]
12. Mitchell, A.L.; Rosenqvist, A.; Mora, B. Current Remote Sensing Approaches to Monitoring Forest Degradation in Support of Countries Measurement, Reporting and Verification (MRV) Systems for REDD+. *Carbon Balance Manag.* **2017**, *12*, 9. [CrossRef]
13. Folega, F.; Zhang, C.; Zhao, X.; Wala, K.; Batawila, K.; Huang, H.; Dourma, M.; Akpagana, K. Satellite Monitoring of Land-Use and Land-Cover Changes in Northern Togo Protected Areas. *J. For. Res.* **2014**, *25*, 385–392. [CrossRef]
14. Akakpo, K.M.; Quensière, J.; Gadal, S.; Kossi, A.; Kokou, K. Caractérisation et Dynamique Spatiale de La Couverture Végétale Dans Les Aires Protégées Du Togo: Étude Par Télédétection Satellitaire de La Forêt Classée de Missahoé Dans La Région Des Plateaux. *Rev. Int. De Géomatique Aménagement Et Gest. Des Ressour.* **2017**, *1*, 181–194.
15. Atsri, H.K.; Konko, Y.; Cuni-Sanchez, A.; Abotsi, K.E.; Kokou, K. Changes in the West African Forest-Savanna Mosaic, Insights from Central Togo. *PLoS ONE* **2018**, *13*, e020399. [CrossRef]
16. Polo-Akpisso, A.; Wala, K.; Soulemane, O.; Folega, F.; Akpagana, K.; Tano, Y. Assessment of Habitat Change Processes within the Oti-Keran-Mandouri Network of Protected Areas in Togo (West Africa) from 1987 to 2013 Using Decision Tree Analysis. *Science* **2020**, *2*, 1. [CrossRef]
17. Badjana, H.M.; Helmschrot, J.; Selsam, P.; Wala, K.; Flügel, W.-A.; Afouda, A.; Akpagana, K. Land Cover Changes Assessment Using Object-Based Image Analysis in the Binah River Watershed (Togo and Benin). *Earth Space Sci.* **2015**, *2*, 403–416. [CrossRef]
18. Diwediga, B.; Agodzo, S.; Wala, K.; Le, Q.B. Assessment of Multifunctional Landscapes Dynamics in the Mountainous Basin of the Mo River (Togo, West Africa). *J. Geogr. Sci.* **2017**, *27*, 579–605. [CrossRef]
19. Koumoi, Z.; Boukpessi, T.; Kpedenou, K.D. Principaux Facteurs Explicatifs de La Dynamique de l'occupation Du Sol Dans Le Centre-Togo: Apport Des SIG et Des Statistiques Spatiales. *Rev. Ivoir. Géographie Savanes* **2017**, *3*, 252–273.
20. Koglo, Y.S.; Gaiser, T.; Agyare, W.A.; Sogbedji, J.M.; Kouami, K. Implications of Some Major Human-Induced Activities on Forest Cover Using Extended Change Matrix Quantity and Intensity Analysis Based on Historical Landsat Data from the Kloto District, Togo. *Ecol. Indic.* **2019**, *96*, 628–634. [CrossRef]
21. Folega, F.; Woegan, Y.A.; Marra, D.; Wala, K.; Batawila, K.; Seburanga, J.L.; Zhang, C.; Peng, D.; Zhao, X.; Akpagana, K. Long Term Evaluation of Green Vegetation Cover Dynamic in the Atacora Mountain Chain (Togo) and Its Relation to Carbon Sequestration in West Africa. *J. Mt. Sci.* **2015**, *12*, 921–934. [CrossRef]
22. Mastro, P.; Masiello, G.; Serio, C.; Pepe, A. Change Detection Techniques with Synthetic Aperture Radar Images: Experiments with Random Forests and Sentinel-1 Observations. *Remote Sens.* **2022**, *14*, 3323. [CrossRef]
23. Mahdianpari, M.; Jafarzadeh, H.; Granger, J.E.; Mohammadimanesh, F.; Brisco, B.; Salehi, B.; Homayouni, S.; Weng, Q. A Large-Scale Change Monitoring of Wetlands Using Time Series Landsat Imagery on Google Earth Engine: A Case Study in Newfoundland. *GIScience Remote Sens.* **2020**, *57*, 1102–1124. [CrossRef]
24. Phan, T.N.; Kuch, V.; Lehnert, L.W. Land Cover Classification Using Google Earth Engine and Random Forest Classifier—The Role of Image Composition. *Remote Sens.* **2020**, *12*, 2411. [CrossRef]
25. Souza, C.M.; Shimbo, J.Z.; Rosa, M.R.; Parente, L.L.; Alencar, A.A.; Rudorff, B.F.T.; Hasenack, H.; Matsumoto, M.; Ferreira, L.G.; Souza-Filho, P.W.M.; et al. Reconstructing Three Decades of Land Use and Land Cover Changes in Brazilian Biomes with Landsat Archive and Earth Engine. *Remote Sens.* **2020**, *12*, 2735. [CrossRef]
26. Gorelick, N.; Hancher, M.; Dixon, M.; Ilyushchenko, S.; Thau, D.; Moore, R. Google Earth Engine: Planetary-Scale Geospatial Analysis for Everyone. *Remote Sens. Environ.* **2017**, *202*, 18–27. [CrossRef]
27. Arévalo, P.; Olofsson, P.; Woodcock, C.E. Continuous Monitoring of Land Change Activities and Post-Disturbance Dynamics from Landsat Time Series: A Test Methodology for REDD+ Reporting. *Remote Sens. Environ.* **2020**, *238*, 111051. [CrossRef]
28. REDD+ Togo. *Plan D'actions de Mise En Oeuvre de La Stratégie Nationale de Réduction Des Émissions Dues à La Déforestation et à La Dégradation Des Forêts (REDD+) 2020–2029*; Coordination Nationale REDD+ du Togo: Lomé, Togo, 2020.

29. INSEED et AFRISTAT. *Enquête Régionale Intégrée Sur l'Emploi et Le Secteur Informel*; 2017; Institut National de la Statistique et des Etudes Economiques et Démographiques et AFRISTAT: Lomé, Togo; Bamako, Mali, 2019; p. 73.
30. PANA. *Plan d'Action National d'Adaptation Au Changement Climatique*; Ministère de l'Environnement et des Ressources Forestières (MERF): Lomé, Togo, 2009; p. 113.
31. REDD+ Togo. *Définition et Calcul Du Taux National de Défloration Annuel Du Togo Entre 1990 et 2015*; Coordination Nationale REDD+ du Togo: Lomé, Togo, 2018.
32. REDD+ Togo. *Étude Sur Les Causes et Conséquences de La Déforestation et La Dégradation Des Forets Au Togo et Identification Des Axes d'intervention Appropries*; Coordination Nationale REDD+ du Togo: Lomé, Togo, 2018.
33. Ern, H. Die Vegetation Togos. Gliederung, Gefährdung, Erhaltung. *Willdenowia* **1979**, *9*, 295–312.
34. MEDDPN. *Analyse Cartographique de l'occupation Des Zones Agroécologiques et Bassins de Concentration Des Populations Au Togo, Folega F., Consultant Sous Ordre de La Coordination Nationale Sur Les Changements Climatiques*; MEDDPN: Lomé, Togo, 2019; p. 66.
35. Brabant, P.; Darracq, S.; Egué, K.; Simonneaux, V.; Aing, A.; Auberton-Habert, E. Togo: État de Dégradation Des Terres Résultant Des Activités Humaines (Note Explicative de La Carte Au 1: 500 000 Des Indices de Dégradation). In *Notice Explicative*; Éditions de I'ORSTOM: Paris, France, 1996; p. 66. ISBN 2-7099-1 348-8.
36. Atakpama, W.; Amegnaglo, K.; Afelu, B.; Folega, F.; Batawila, K.; Akpagana, K. Biodiversité et biomasse pyrophyte au Togo. *Vertigo* **2019**, *19*, 22. [CrossRef]
37. Alboabidallah, A.; Martin, J.; Lavender, S.; Abbott, V. Using Landsat-8 and Sentinel-1 Data for Above Ground Biomass Assessment in the Tamar Valley and Dartmoor. In Proceedings of the 2017 9th International Workshop on the Analysis of Multitemporal Remote Sensing Images (MultiTemp), Bruges, Belgium, 27–29 June 2017; IEEE: Piscataway Township, NJ, USA, 2017; pp. 1–7.
38. Wulder, M.A.; Loveland, T.R.; Roy, D.P.; Crawford, C.J.; Masek, J.G.; Woodcock, C.E.; Allen, R.G.; Anderson, M.C.; Belward, A.S.; Cohen, W.B.; et al. Current Status of Landsat Program, Science, and Applications. *Remote Sens. Environ.* **2019**, *225*, 127–147. [CrossRef]
39. Hu, Y.; Hu, Y. Land Cover Changes and Their Driving Mechanisms in Central Asia from 2001 to 2017 Supported by Google Earth Engine. *Remote Sens.* **2019**, *11*, 554. [CrossRef]
40. Xie, S.; Liu, L.; Zhang, X.; Yang, J.; Chen, X.; Gao, Y. Automatic Land-Cover Mapping Using Landsat Time-Series Data Based on Google Earth Engine. *Remote Sens.* **2019**, *11*, 3023. [CrossRef]
41. Griffiths, P.; van der Linden, S.; Kuemmerle, T.; Hostert, P. A Pixel-Based Landsat Compositing Algorithm for Large Area Land Cover Mapping. *IEEE J. Sel. Top. Appl. Earth Obs. Remote Sens.* **2013**, *6*, 2088–2101. [CrossRef]
42. Zhu, Z.; Woodcock, C.E. Continuous Change Detection and Classification of Land Cover Using All Available Landsat Data. *Remote Sens. Environ.* **2014**, *144*, 152–171. [CrossRef]
43. Hermosilla, T.; Wulder, M.A.; White, J.C.; Coops, N.C.; Hobart, G.W. Disturbance-Informed Annual Land Cover Classification Maps of Canada's Forested Ecosystems for a 29-Year Landsat Time Series. *Can. J. Remote Sens.* **2018**, *44*, 67–87. [CrossRef]
44. Giovos, R.; Tassopoulos, D.; Kalivas, D.; Lougkos, N.; Priovolou, A. Remote Sensing Vegetation Indices in Viticulture: A Critical Review. *Agriculture* **2021**, *11*, 457. [CrossRef]
45. Sozzi, M.; Kayad, A.; Marinello, F.; Taylor, J.; Tisseyre, B. Comparing Vineyard Imagery Acquired from Sentinel-2 and Unmanned Aerial Vehicle (UAV) Platform. *Oeno One* **2020**, *54*, 189–197. [CrossRef]
46. Li, Y.; Zhao, Z.; Xin, Y.; Xu, A.; Xie, S.; Yan, Y.; Wang, L. How Are Land-Use/Land-Cover Indices and Daytime and Nighttime Land Surface Temperatures Related in Eleven Urban Centres in Different Global Climatic Zones? *Land* **2022**, *11*, 1312. [CrossRef]
47. Khan, M.S.; Ullah, S.; Chen, L. Comparison on Land-Use/Land-Cover Indices in Explaining Land Surface Temperature Variations in the City of Beijing, China. *Land* **2021**, *10*, 1018. [CrossRef]
48. Xue, J.; Su, B. Significant Remote Sensing Vegetation Indices: A Review of Developments and Applications. *J. Sens.* **2017**, *2017*, 1353691. [CrossRef]
49. McFeeters, S.K. The Use of the Normalized Difference Water Index (NDWI) in the Delineation of Open Water Features. *Int. J. Remote Sens.* **1996**, *17*, 1425–1432. [CrossRef]
50. Vaudour, E.; Gomez, C.; Lagacherie, P.; Loiseau, T.; Baghdadi, N.; Urbina-Salazar, D.; Loubet, B.; Arrouays, D. Temporal Mosaicking Approaches of Sentinel-2 Images for Extending Topsoil Organic Carbon Content Mapping in Croplands. *Int. J. Appl. Earth Obs. Geoinf.* **2021**, *96*, 102277. [CrossRef]
51. Xu, N.; Tian, J.; Tian, Q.; Xu, K.; Tang, S. Analysis of Vegetation Red Edge with Different Illuminated/Shaded Canopy Proportions and to Construct Normalized Difference Canopy Shadow Index. *Remote Sens.* **2019**, *11*, 1192. [CrossRef]
52. Chen, Y.; Cao, R.; Chen, J.; Liu, L.; Matsushita, B. A Practical Approach to Reconstruct High-Quality Landsat NDVI Time-Series Data by Gap Filling and the Savitzky–Golay Filter. *ISPRS J. Photogramm. Remote Sens.* **2021**, *180*, 174–190. [CrossRef]
53. Huang, S.; Tang, L.; Hupy, J.P.; Wang, Y.; Shao, G. A Commentary Review on the Use of Normalized Difference Vegetation Index (NDVI) in the Era of Popular Remote Sensing. *J. For. Res.* **2021**, *32*, 1–6. [CrossRef]
54. Özelkan, E. Water Body Detection Analysis Using NDWI Indices Derived from Landsat-8 OLI. *Pol. J. Environ. Stud.* **2020**, *29*, 1759–1769. [CrossRef]
55. Rikimaru, A.; Roy, P.S.; Miyatake, S. Tropical Forest Cover Density Mapping. *Trop. Ecol.* **2002**, *43*, 39–47.
56. Zheng, Y.; Tang, L.; Wang, H. An Improved Approach for Monitoring Urban Built-up Areas by Combining NPP-VIIRS Nighttime Light, NDVI, NDWI, and NDBI. *J. Clean. Prod.* **2021**, *328*, 129488. [CrossRef]

57. Nyland, K.E.; Gunn, G.I.; Shiklomanov, N.N.; Engstrom, R.A.; Streletskiy, D. Land Cover Change in the Lower Yenisei River Using Dense Stacking of Landsat Imagery in Google Earth Engine. *Remote Sens.* **2018**, *10*, 1226. [CrossRef]
58. Tian, S.; Zhang, X.; Tian, J.; Sun, Q. Random Forest Classification of Wetland Landcovers from Multi-Sensor Data in the Arid Region of Xinjiang, China. *Remote Sens.* **2016**, *8*, 954. [CrossRef]
59. Wingate, V.R.; Phinn, S.R.; Kuhn, N.; Bloemertz, L.; Dhanjal-Adams, K.L. Mapping Decadal Land Cover Changes in the Woodlands of North Eastern Namibia from 1975 to 2014 Using the Landsat Satellite Archived Data. *Remote Sens.* **2016**, *8*, 681. [CrossRef]
60. Zurqani, H.A.; Post, C.J.; Mikhailova, E.A.; Schlautman, M.A.; Sharp, J.L. Geospatial Analysis of Land Use Change in the Savannah River Basin Using Google Earth Engine. *Int. J. Appl. Earth Obs. Geoinf.* **2018**, *69*, 175–185. [CrossRef]
61. Fernández-Delgado, M.; Cernadas, E.; Barro, S.; Amorim, D. Do We Need Hundreds of Classifiers to Solve Real World Classification Problems? *J. Mach. Learn. Res.* **2014**, *15*, 3133–3181.
62. Zhang, D.-D.; Zhang, L. Land Cover Change in the Central Region of the Lower Yangtze River Based on Landsat Imagery and the Google Earth Engine: A Case Study in Nanjing, China. *Sensors* **2020**, *20*, 2091. [CrossRef] [PubMed]
63. Probst, P.; Boulesteix, A.-L. To Tune or Not to Tune the Number of Trees in Random Forest. *J. Mach. Learn. Res.* **2017**, *18*, 6673–6690.
64. Oshiro, T.M.; Perez, P.S.; Baranauskas, J.A. How Many Trees in a Random Forest? In Proceedings of the Machine Learning and Data Mining in Pattern Recognition, New York, NY, USA, 30 August–3 September 2011; Perner, P., Ed.; Springer: Berlin/Heidelberg, Germany, 2012; pp. 154–168.
65. Probst, P.; Wright, M.N.; Boulesteix, A.-L. Hyperparameters and Tuning Strategies for Random Forest. *WIREs Data Min. Knowl. Discov.* **2019**, *9*, e1301. [CrossRef]
66. Guo, L.; Ma, Y.; Cukic, B.; Singh, H. Robust Prediction of Fault-Proneness by Random Forests. In Proceedings of the 15th International Symposium on Software Reliability Engineering, Saint-Malo, France, 2–5 November 2004; pp. 417–428.
67. Gislason, P.O.; Benediktsson, J.A.; Sveinsson, J.R. Random Forests for Land Cover Classification. *Pattern Recognit. Lett.* **2006**, *27*, 294–300. [CrossRef]
68. Bernard, S.; Adam, S.; Heutte, L. Dynamic Random Forests. *Pattern Recognit. Lett.* **2012**, *33*, 1580–1586. [CrossRef]
69. Kulkarni, A.; Lowe, B. Random Forest Algorithm for Land Cover Classification. *Comput. Sci. Fac. Publ. Present.* **2016**, *4*, 58–63.
70. Lind, A.P.; Anderson, P.C. Predicting Drug Activity against Cancer Cells by Random Forest Models Based on Minimal Genomic Information and Chemical Properties. *PLoS ONE* **2019**, *14*, e0219774. [CrossRef]
71. MERF. *Rapport Inventaire Forestier National Du Togo 2015–2016*; Ministère de l'Environnement et des Ressources Forestières (MERF): Lomé, Togo, 2016; p. 79.
72. Verma, P.; Raghubanshi, A.; Srivastava, P.K.; Raghubanshi, A.S. Appraisal of Kappa-Based Metrics and Disagreement Indices of Accuracy Assessment for Parametric and Nonparametric Techniques Used in LULC Classification and Change Detection. *Model. Earth Syst. Environ.* **2020**, *6*, 1045–1059. [CrossRef]
73. Petropoulos, G.P.; Kalivas, D.P.; Georgopoulou, I.A.; Srivastava, P.K. Urban Vegetation Cover Extraction from Hyperspectral Imagery and Geographic Information System Spatial Analysis Techniques: Case of Athens, Greece. *J. Appl. Remote Sens.* **2015**, *9*, 096088. [CrossRef]
74. Tang, H.; Hu, Z. Research on Medical Image Classification Based on Machine Learning. *IEEE Access* **2020**, *8*, 93145–93154. [CrossRef]
75. Congedo, L. Semi-Automatic Classification Plugin: A Python Tool for the Download and Processing of Remote Sensing Images in QGIS. *J. Open Source Softw.* **2021**, *6*, 3172. [CrossRef]
76. Puyravaud, J.-P. Standardizing the Calculation of the Annual Rate of Deforestation. *For. Ecol. Manag.* **2003**, *177*, 593–596. [CrossRef]
77. Lopes, M.; Frison, P.-L.; Crowson, M.; Warren-Thomas, E.; Hariyadi, B.; Kartika, W.D.; Agus, F.; Hamer, K.C.; Stringer, L.; Hill, J.K.; et al. Improving the Accuracy of Land Cover Classification in Cloud Persistent Areas Using Optical and Radar Satellite Image Time Series. *Methods Ecol. Evol.* **2020**, *11*, 532–541. [CrossRef]
78. Feyisa, G.L.; Meilby, H.; Fensholt, R.; Proud, S.R. Automated Water Extraction Index: A New Technique for Surface Water Mapping Using Landsat Imagery. *Remote Sens. Environ.* **2014**, *140*, 23–35. [CrossRef]
79. Wijedasa, L.S.; Sloan, S.; Michelakis, D.G.; Clements, G.R. Overcoming Limitations with Landsat Imagery for Mapping of Peat Swamp Forests in Sundaland. *Remote Sens.* **2012**, *4*, 2595–2618. [CrossRef]
80. Masiello, G.; Cersosimo, A.; Mastro, P.; Serio, C.; Venafra, S.; Pasquariello, P. Emissivity-Based Vegetation Indices to Monitor Deforestation and Forest Degradation in the Congo Basin Rainforest. In Proceedings of the Remote Sensing for Agriculture, Ecosystems, and Hydrology XXII, Online, 20 September 2020; SPIE: Bellingham, WA, USA, 2020; Volume 11528, pp. 125–138.
81. Dong, J.; Xiao, X.; Menarguez, M.A.; Zhang, G.; Qin, Y.; Thau, D.; Biradar, C.; Moore, B. Mapping Paddy Rice Planting Area in Northeastern Asia with Landsat 8 Images, Phenology-Based Algorithm and Google Earth Engine. *Remote Sens. Environ.* **2016**, *185*, 142–154. [CrossRef] [PubMed]